**Geoscientific
Model Development
Discussions**

y

Geoscientific Model Development Discussions is the access reviewed
discussion forum of *Geoscientific Model Development*

ECHMERIT V1.0 – a new global fully coupled mercury-chemistry and transport model

G. Jung, I. M. Hedgecock, and N. Pirrone

CNR – Institute for Atmospheric Pollution, Division of Rende, 87036 Rende, Italy

Correspondence to: G. Jung (g.jung@cs.iia.cnr.it)

ECHMERIT model

G. Jung et al.

Title Page

Abstract	Introduction
Conclusions	References
Tables	Figures

|◄|►|

|◄|►|

Back | Close

Full Screen / Esc

Printer-friendly Version

Interactive Discussion

Abstract

Mercury is a global pollutant due to its long lifetime in the atmosphere. Its hemispheric transport patterns and eventual deposition are therefore of major concern. For the purpose of global atmospheric mercury chemistry and transport modelling the ECHMERIT
5 model was developed. ECHMERIT, based on the global circulation model ECHAM5 differs from most global mercury models in that the emissions, chemistry (including general tropospheric chemistry and mercury chemistry), transport and deposition are coupled on-line to the GCM. The chemistry mechanism includes an online calculation of photolysis rate constants using the Fast-J photolysis mechanism, the CBM-Z tropo-
10 spheric gas-phase mechanism and aqueous-phase chemistry based on the MECCA mechanism. Additionally, a mercury chemistry mechanism that incorporates gas and aqueous phase mercury chemistry is included. A detailed description of the model, including the wet and dry deposition modules, and the implemented emissions is given in this technical report. First model testing and evaluation show a satisfactory model per-
15 formance for surface ozone and mercury concentrations (with a mean bias of 1.46 ppb for ozone and a mean bias of 13.55 ppq for TGM when compared with EMEP station data). Requirements regarding measurement data and emission inventories which could considerably improve model skill are discussed.

1 Introduction

20 While local and regional emission sources are the main cause of air pollution problems worldwide, there is increasing evidence that many air pollutants are transported on a hemispheric or global scale and are hence altering air quality even in remote areas (Stohl et al., 2002; Liang et al., 2004; Eckhardt et al., 2003; Lindberg et al., 2007). Mercury is a global pollutant because in its elemental form it reacts relatively slowly
25 with the most abundant atmospheric oxidants and is therefore transported far from its emission source. In fact the background concentration of Hg at the poles is similar

to that in rural areas of Europe (Sprovieri et al., 2002). Additionally, mercury is of public concern, as it bioaccumulates, which can lead to very high levels of mercury compounds, especially in predators, at the end of the food chain (Lubick, 2009).

A recent summary of current knowledge on mercury emissions, chemistry and also
5 modelling can be found in the interim report of the UNEP Global Partnership on Atmospheric Mercury Transport and Fate Research (Pirrone and Mason, 2008).

Mercury is released to the atmosphere from a variety of natural sources, such as volcanoes, surface waters, soil and vegetation, as well as from anthropogenic sources, particularly fossil fuel combustion, processing of mineral resources, chlor-alkali plants
10 and waste incineration (Pirrone et al., 1996; Schroeder et al., 1998; Pacyna et al., 2006). Subsequently mercury is subject to chemical transformation, atmospheric transport, wet and dry deposition and potential bioaccumulation in the biosphere. Emissions from water bodies are estimated to be 2778 Mg y^{-1} according to Pirrone and Mason (2009), which is 33% of the total Hg emissions to the atmosphere. Including all natural
15 sources (volcanic activity, vegetation, soils, rocks, forest fires and oceans) results in annual global emissions of 5207 Mg, whereas the sum of anthropogenic emissions is estimated to be about 2503 Mg y^{-1} (Pirrone and Mason, 2009). Of the natural emissions, only one third is assumed to be not influenced by past anthropogenic activities at all. The other two-thirds of the "natural" emissions are considered to be re-emission
20 of previously deposited Hg resulting from anthropogenic activity. Nevertheless, distinguishing between natural emissions of mercury and mercury which was previously deposited and is re-emitted from land surfaces, vegetation and water bodies is hardly possible (Pirrone et al., 1996).

Three types of mercury species are measured in the atmosphere. Elemental mer-
25 cury, which is almost insoluble makes up the major part of the atmospheric Hg reservoir (95–99%), whereas reactive gaseous mercury (RGM) is about 3% of the amount of elemental mercury (Bullock, 2000). RGM is an operationally defined term which refers to oxidised compounds which are collected on KCl denuders, and detected as elemental mercury (Hg^0) after thermal reduction and desorption. Oxidised Hg compounds

Printer-friendly Version

Interactive Discussion

are more chemically reactive and soluble than elemental mercury, and therefore easily scavenged in cloud droplets where they can take part in aqueous phase reactions. RGM is therefore also more strongly affected by wet and dry deposition processes than the less reactive and less soluble elemental mercury. Hence, even though it is the less abundant of the gas phase atmospheric Hg species, RGM is responsible for the major part of Hg removal from the atmosphere. RGM is assumed to include gaseous Hg^{II} compounds such as $HgCl_2$, HgO or $HgBr_2$ (compare to the discussion in chapter 2.3). Mercury associated with particulate matter (Hg_p) is also found in the atmosphere, and is deposited but makes up only about 0.2–1.4% of total atmopheric Hg (Ebinghaus et al., 2008). Hg_p is either primary particulate matter or condensed Hg compounds, or semi-volatile Hg bound to aerosols. The different chemical and physical characteristics of Hg species greatly influence their atmospheric lifetime. Because RGM is rapidly removed from the atmosphere it has a resulting lifetime in the order of days to weeks. Elemental Hg is in contrast, due to its long lifetime of 0.5–2 years (Hedgecock and Pirrone, 2004), transported over long distances. This means also that the relationship between emissions, atmospheric concentrations, and deposition is much less straightforward, than for shortlived chemical species, and hence interhemispheric transport plays a major role in mercury chemistry modelling.

Mercury concentrations and gradients are rather constant in both hemispheres, with background values of total gaseous mercury (TGM, the sum of RGM and Hg^0) of around 1.1–1.3 ng m^{-3} in the Southern and 1.5 to 1.7 ng m^{-3} in the Northern Hemisphere (Lindberg et al., 2007)

The enhancement of mercury emissions starting with industrialization led to an increase in mercury concentrations by a factor of three, compared to pre-industrial times (Lindberg et al., 2007). In the lower troposphere and in surface levels Hg concentrations decreased from the late 1980's to 1990's (Slemr et al., 2003). Observations at Mace Head, a background station in Ireland, demonstrated almost constant concentrations from 1995 to 2001 (Ebinghaus et al., 2002), whereas observations on the Wank summit in Germany and over the Atlantic Ocean by Slemr and Scheel (1998) even

showed a decrease over the entire 1990s. European emissions show a decrease of a factor of more than 4 from 1980 to 2005, but for the years from 2003 to 2005 a strong increase in mercury concentrations, in air, but also in precipitation can be observed for Europe, which is most likely due to the recent emission growth in the developing
5 economies of South and East Asia (Pacyna et al., 2009).

To investigate not only chemical transformation processes, but also the influence of long-range transport on the global and continental distribution of mercury concentrations, hemispheric and global mercury-chemistry models had to be developed. Not many atmospheric mercury chemistry and transport models exist so far.

10 On the hemispheric scale, the Danish Eulerian Hemispheric Model (DEHM) (Christensen et al., 2004) was used to investigate the mercury cycle and concentrations in the Northern Hemisphere, with a special focus on arctic mercury depletion events. DEHM is an offline, eulerian model where mercury chemistry includes gas and aqueous phase chemistry, as well as fast oxidation at polar sunrise.

15 Another offline large-scale model, working on the hemispheric scale, is the MSCE-Hg-Hem (Travnikov, 2005), of the Meteorological Synthesizing Centre East, Moscow. It runs at a relatively coarse resolution with 8 vertical layers and a horizontal resolution of 2.5°. It includes gas and acqueous phase oxidation by O_3, chlorine, OH and aqueous-phase reduction via decomposition of sulphite complexes, the formation of
20 chloride complexes and adsorption by soot particles in cloud water, where monthly mean concentrations for the reactants are used. For the boundary condition a fixed gradient of elemental mercury concentration is set at the equator. MSCE-Hg-Hem has been widely tested. Investigating hemispheric transport it was demonstrated, that even in industrialized regions, the contribution from intercontinental atmospheric transport is
25 comparable with that of regional emissions.

On the global scale, the mercury chemistry version of the GEOS-chem model (Bey et al., 2001), an offline CTM including mercury chemistry, driven with assimilated meteorological data from the Goddard Earth Observing System (GEOS) of the NASA Data Assimilation Office (DAO) demonstrated reasonable results in reproducing mer-

◄◄ | ►►

◄ | ►

Back | Close

Full Screen / Esc

cury concentrations and concentration gradients in both hemispheres. GEOS-chem for Hg has so far been run in a resolution of 4×5° and 30 vertical levels and is coupled to a mixed-layer slab ocean model. It includes oxidation by OH and O_3 in the gas phase and photochemical reduction in clouds.

CTM-Hg (Global Chemical Transport Model for Mercury) developed by AER/EPRI (Atmospheric and Environmental Research, Inc./Electric Power Research Institute) (Seigneur et al., 2001, 2004) is another global scale offline model that runs with a resolution of 8×10° and nine vertical layers but has a rather complex chemistry included, that considers gas- and aqueous-phase oxidation and aqueous-phase reduction of Hg species. The sensitivity of CTM-Hg to the chemical mechanism and specific reaction rate constants (Seigneur et al., 2006, 2003), as well as to emissions (Lohman et al., 2008) has been extensively tested. These studies showed the strong impact of the choice of reactions and rate constants, as well as the impact of anthropogenic, natural and re-emissions on the global distribution of mercury in the atmosphere and stress the need for further research in the field of mercury chemistry, as well as in observations, emission inventories and hence model development.

To date, only the GRAHM (Global/Regional Atmospheric Heavy Metals) model (Dastoor and Larocque, 2004) is run in a directly coupled online mode with respect to meteorology. This model incorporates a variable grid resolution, and proved its ability to represent seasonal variability and the latitudinal gradient of mercury concentrations. No ozone photochemistry is modelled in GRAHM, ozone fields are instead received from monthly averaged MOZART (Horowitz et al., 2003) simulations. Within the complex mercury chemistry mechanism, oxidation by halogen species in the marine boundary layer and polar regions is included.

The newly developed model ECHMERIT, that is presented in the following is designed to combine the advantages of an online-coupling approach for atmospheric chemistry and transport modelling with a rather complex tropospheric chemistry and mercury chemistry description, suitable for global scale issues and flexible enough to be run in low to high resolution.

ECHMERIT model

G. Jung et al.

⏮ | ⏭

◀ | ▶

Back | Close

Full Screen / Esc

Printer-friendly Version

Interactive Discussion

2 Model description

ECHMERIT is a fully coupled model, based on the Atmospheric General Circulation Model *ECH*AM5, and a *MER*cury chemistry module, developed at the Institute for Atmospheric Pollution of the Italian National Research Council (CNR-IIA) in Rende, *IT*aly.

2.1 Atmospheric physics

The atmospheric physics part of the global-scale model ECHMERIT is based on the fifth generation global climate model ECHAM5, which is developed and maintained at the Max-Planck Institute for Meteorology in Hamburg/Germany. ECHAM5 has been widely used to investigate atmospheric responses to various greenhouse-gas emission scenarios, and model performance has been extensively tested (Roeckner et al., 2003, 2005). A flexible nudging routine that is implemented in ECHAM5 enables the model to be run under real meteorological conditions for long-term simulations, nudging the model results to global reanalyses.

The basic prognostic variables of ECHAM5 are vorticity, divergence, temperature, logarithm of surface pressure and the mixing ratios of the various moisture components (like cloud water, rain water, cloud ice).

Shortwave radiation is calculated in a 2 h time step, for four spectral bands, one for visible and UV range and three for the near infrafred. It includes an annual, as well as a diurnal cycle of solar forcing. Absorption due to water vapor and ozone are taken into account, as well as absorption due to CO_2, N_2O, CO, CH_4 and O_2 as uniformly mixed gases. Scattering due to aerosols following the Mie-theory using idealized distributions of cloud ice and droplets and Rayleigh scattering are considered as well.

Gridscale cloud water content and cloud ice content are calculated from the respective budget equation, including transport of cloud water and a simplified representation of microphysical processes such as condensation, evaporation, formation of cloud droplets through coalescence, and sedimentation of ice crystals. Sub-gridscale cloud formation is also parameterized, dependent on fluctuations in total water content. The

ECHMERIT model

G. Jung et al.

bulk mass flux scheme of Tiedtke (1989) with modifications after Nordeng (1994) is used to represent convective mass fluxes. Deep, mid level and shallow convection are considered. Organized entrainment is calculated from buoyancy, organized detrainment is computed from a spectrum of clouds detraining at different heights. Cloud water detrainment in the upper part of the convective updrafts is a source term in the stratiform cloud water equations. For deep convection an adjustment-type closure is used, which relates the cloud base mass flux to convective instability.

A parameterization for the representation of sub-gridscale orographic effects on atmospheric dynamics following Lott and Miller (1997) is included.

The soil and land surface model comprises the budgets of soil heat and water, snow cover and the heat budget of land ice. It takes into consideration the stomatal control of surface evapotranspiration through vegetation, interception, and the dependence of the sensible heat flux on snow coverage in a highly parameterized form. Major land surface properties are given as fractional values with respect to the forest, sea, snow and sea-ice fraction of a grid cell. The land-surface parameters were derived from Hagemann (2002).

2.2 Transport

In the base model ECHAM5 a tracer transport routine is already implemented, for passive tracer variables, as well as water vapour. Tracers are transported through advection, convection and vertical diffusion. For transport due to advection the flux-form semi-Lagrangian advection scheme of Lin and Rood (1996) was chosen. This tracer transport scheme is a semi-Lagrangian extension of a flux-form scheme. It ensures local and global mass conservation and preserves linear tracer correlations.

The scheme of Tiedtke (1989) and Nordeng (1994), as implemented in ECHAM5 is used to calculate convective mass transport. A mass flux correction had to be implemented in ECHMERIT, because negative concentration values can occur in the case of strong gradients of tracer concentrations in the convective transport calculation. This especially happens in the lowest model layers, near source regions and affects most of

all species with low background values but relatively large emissions. The implemented correction is strictly mass conserving and positive definite. In case net fluxes out of a grid cell exceed the available tracer mass within that cell, the fluxes are restricted to the maximum value of the available tracer as described in the following.

5   Mass fluxes that contribute to the updating of tracer tendencies after the calculation of convective fluxes of a single grid cell in level k are: F_{up}^k and F_{up}^{k+1}, the convective updraft fluxes out of the respective layer and entering from the layer below and F_{down}^k and F_{down}^{k+1} the downdraft from the layer above and to the layer below.

The calculation of mass flux correction is performed successively from the lowest
10 layer to the top layer in such a way that only the respective fluxes that enter and leave a cell at the top boundary are taken into consideration for correction within one grid cell. First at the end of the convection routine, the new tracer tendencies are calculated. In case the tracer mass flux exceeds the tracer concentration of a grid cell, the correction scheme is applied. With *TM*, the excessive tracer mass flux, the correction factor (*CR*)
15 is therefore calculated as:

$$CR = \frac{TM}{(F_{up}^k + F_{down}^k)} \qquad (1)$$

This correction factor is then used to calculated the corrected mass fluxes *F*new.

$$F\text{new}_{up}^k = F_{up}^k \times CR \qquad (2)$$

$$F\text{new}_{down}^k = F_{down}^k \times CR \qquad (3)$$

20 Fluxes that enter and exit the cell above at the lower boundary are then updated accordingly and correction for the successive layer is continued if necessary. This scheme does not only make sure that the values are restricted to non-negative tracer concentrations, which could be also achieved by a simple cut-off of negative values, but also conserves the tracer mass of the respective model column. Nevertheless this
25 is a relatively simple approach, which will in future model development be replaced by

Full Screen / Esc

Printer-friendly Version

Interactive Discussion

a more complex correction scheme such as that proposed for the Tiedtke-scheme by Brinkop and Sausen (1997).

In ECHMERIT the following 26 species (Table 1) are transported and deposited. $Hg^{II}(aq)$ is a lumped species including all aqueous-phase mercury species present
₅ in the chemistry mechanism of ECHMERIT. For transport calculation these species are all lumped to the one species $Hg^{II}(aq)$. After transport and deposition, before the next chemistry calculation all present $Hg^{II}(aq)$ is transferred to $Hg^{++}(aq)$ which then complexes rapidly with available ligands. When a grid cell in the next time step turns out to have a very low water content and hence only gas-phase chemistry will be
₁₀ calculated, the contained $Hg^{II}(aq)$ is assumed to be solid and is not subject to chemical processes, but to transport. If it later enters a "wet" grid cell it is again scavenged to take part in aqueous phase chemistry.

2.3 Chemistry

A wide range of different chemistry mechanisms exist in atmospheric chemistry mod-
₁₅ elling, with a great variety of complexity. Due to the largely different lifetimes of the chemical species involved, the numerical integration of these chemistry mechanisms results in highly coupled, extremely stiff non-linear systems of ordinary differential equations that require major computational effort to solve. Therefore, for application in a global atmospheric pollution and transport study it is not feasible to choose a de-
₂₀ tailed mechanism including a too large a number of chemical species and reactions. Instead, in most commonly applied coupled meteorology-chemistry, but also in chemical transport models the chemical mechanisms incorporate lumped chemical species to represent various species with similar lifetimes and/or chemical behaviour.

The chemistry module in ECHMERIT treats gas phase reactions, aqueous phase
₂₅ reactions, exchange of compounds between the aqueous and gas phases and photolysis reactions all in one overall chemical mechanism. The module was prepared using the Kinetic Pre-Processor (version 2.1) (Damina-Iordache et al., 2002).

Back | Close

Full Screen / Esc

Printer-friendly Version

Interactive Discussion

The gas phase chemical mechanism is based on the CBM-Z mechanism (Zaveri and Peters, 1999). The CBM-Z mechanism is a follow-up to the CBM-IV mechanism, with revised inorganic and peroxide chemistry, that was specifically optimised to be suitable for longer temporal and larger spatial scales than was originally envisaged for CBM-
5 IV. To achieve that purpose some longer-lived species and their intermediates were included, to provide a better representation of long-range transport of air pollutants.

The tropospheric aqueous phase mechanism is derived from MECCA (Sander et al., 2005) and treats O_x, HO_x, NO_x, NH_3, CO_2 and SO_x chemistry.

In the model the exchange of soluble compounds between the gas and aqueous
10 phases is included as a forward and backward reaction. Equilibrium between the two phases is not assumed. (The same approach is used for aqueous phase equilibria.) The rate of uptake of a soluble gas is described by a mass transfer coefficient using the approach of Schwartz (1986):

$$k_{mt} = (\frac{r^2}{3D_g} + \frac{4r}{3\bar{v}\alpha})^{-1} \tag{4}$$

15 where k_{mt} is the mass transfer coefficient in [s^{-1} m_{air}^3 m_{aq}^{-3}], r is the mean droplet radius, D_g the gas phase diffusivity, $\bar{v}$ is the mean molecular velocity and α is the accommodation coefficient. The rate of uptake is then proportional to the mass transfer coefficient and the liquid water content and how far the aqueous phase concentration is from equilibrium as defined by the Henry's Law constant, see Sander (1999).

20 The general tropospheric chemistry equations and equilibria that are based on the CBM-Z and the MECCA mechanisms and the respective references for chosen rate constants are summarized in Appendix A.

For calculation of the rate constants for photolysis reactions, the Fast-J photolysis mechanism (Wild et al., 2000) was included. The photolysis routine is called and pho-
25 tolysis rate constants are updated every chemistry time step.

Due to the interest in Hg as a global pollutant, its gas phase chemistry in the atmosphere has recently been the subject of much study. The low vapour pressure of

ECHMERIT model

G. Jung et al.

elemental Hg and the fact that oxidised Hg compounds are solids at room temperature lead to a number of experimental difficulties when attempting to determine reaction rate constants. There is some debate still as to whether certain oxidation reactions, particularly those which would lead to the formation of HgO actually occur in the gas phase under atmospheric conditions at all. It is possible that reactions between Hg and OH and between Hg and O_3 would require the presence of a surface (Hynes et al., 2008; Ariya et al., 2008).

The reaction products of the gas phase oxidation of Hg have not been definitively identified in reaction rate studies, nor have they been isolated in the atmosphere itself. The common term used to describe oxidised gas phase mercury compounds is Reactive Gaseous Mercury (RGM) which is operationally defined. Compounds collected on a KCl (potassium chloride) denuder usually over a period of two or four hours are then thermally reduced to elemental mercury which is detected using CVAFS (Cold Vapor Atomic Fluorescence Spectrophotometry). In modelling studies the products of the reactions with e.g. O_3, OH and H_2O_2 are generally assumed to be either all particulate or all gas phase. The effects of these assumptions on the modelled RGM concentrations in the Mediterranean MBL assuming either solid or gas phase products has been investigated and compared to measured RGM concentrations using a box model (Hedgecock et al., 2005). In this study it was found that measured RGM in the MBL was best represented either by the slower (Hall, 1995) rate constant for O_3+Hg and assuming the oxidation product to be in the gas phase, or by using the more rapid rate constant (Pal and Ariya, 2004) and assuming that the product was solid, and therefore did not contribute to the RGM concentration. The faster rate for the O_3+Hg reaction is not generally used in global, hemispheric or regional models as it becomes difficult to reproduce the uniformity of the distribution of Hg^0 in the absence of known competing reduction reactions.

The gas phase reactions of Hg which have been added to the CBM-Z mechanism include those with O_3, OH, H_2O_2, HCl, NO_3 and Br. The reactions with Br have been included for future modelling and require a Br/BrO climatology. This is not yet included

in the model. ECHMERIT in line with other global Hg models uses the Hall (1995) value for the Hg+O_3 reaction, and following the discussion above, the oxidised products are assumed to be all in the gas phase. These products are assumed to have the same Henry's Law constant as HgO. Therefore they are readily scavenged in the presence
5 of liquid water and in the following subject to dry, as well as wet deposition to a much larger amount than elemental mercury with its low reactivity and solubility.

To the MECCA aqueous phase mechanism, mercury oxidation by O_3, OH and HOCl/OCl$^-$, complexation with OH$^-$, SO$_3^-$, and Cl$^-$, and reduction via the dissociation of HgSO$_3$ have been added. Many models include the reduction of aqueous phase
10 Hg^{II}, independent of speciation, by dissolved HO$_2$ in a two step reaction which proceeds via Hg^I (Pehkonen and Lin, 1998), however the validity of this reduction mechanism has been called into question because the Hg^I formed in the first step of the reaction would be rapidly re-oxidised by dissolved O_2 (Gårdfeldt and Jonsson, 2003). This reaction has therefore been excluded.
15 The rate constants chosen from the literature for gas, as well as aqueous-phase reactions used in ECHMERIT are summarized in Tables 2 and 3. For a discussion of the relative merits of one rate determination over another the reader is referred to chapters 14 and 15 of the interim report of the UNEP Global Partnership on Atmospheric Mercury Transport and Fate Research (Hynes et al., 2008; Ariya et al., 2008).
20 No atmospheric gas phase reduction reactions are known for Hg compounds although SO$_2$ and CO have been postulated as possible reductants (Vijayaraghavan et al., 2008; Pongprueksa et al., 2007).

The chemistry mechanism implemented in ECHMERIT includes altogether 121 chemical species and represents gas, as well as aqueous-phase chemistry, with a
25 total number of 288 chemical reactions. No stratospheric chemistry is included. To solve the chemical ODE system the variable order stiff extrapolation SEULEX solver, as described in Sandu and Sander (2006) was found to produce reasonable results, and to be more stable than the Rosenbrock solvers of 2nd and 3rd order that were also tested. In order to save computational time and to avoid model instabilities for grid

ECHMERIT model

G. Jung et al.

Printer-friendly Version

Interactive Discussion

cells with a low water content, ECHMERIT distinguishes between wet and dry chemistry in a way that wet chemistry is only called in case of cloud water content exceeding a specific pre-defined threshold value. Therefore in the present model version a minimum value of $10^5\,\mu\mathrm{g\,m^{-3}}$ for running aqueous-phase chemistry, according to Jacobson (1999) was set.

2.4 Deposition

2.4.1 Gaseous dry deposition

For gaseous dry deposition, within ECHMERIT an approach similar to that described by Kerkweg et al. (2006) is used, which applies the big leaf approach used in ECHAM3 and ECHAM4 (Ganzeveld and Lelieveld, 1995; Ganzeveld et al., 1998, 2006), taking into consideration bulk properties of the respective surfaces, without accounting for removal processes occuring in different layers of the canopy. Deposition velocities are calculated from turbulent transfer, vegetation activity and uptake rates on soil, water and snow/ice. Generally the scheme is based on the commonly applied approach first described by Wesely and Hicks (1977).

Thereafter the deposition velocity v_d is calculated using the parallel resistances approach with R_a the aerodynamic resistance, R_b, the boundary layer resistance, and the surface resistance R_s. The calculation of these resistances generally follows Kerkweg et al. (2006).

In ECHMERIT a scaling of all species resistances to those of O_3 and SO_2 as in Wesely (1989) is applied and the calculated resistances depend on the solubility and reactivity of the respective species. This makes the scheme easily extendible to other chemical species. Basic resistance values for O_3 and SO_2 are taken from Kerkweg et al. (2006). The partitioning of land grid cells into fractions of snow/ice, bare soil, water/wet skin and vegetation, that is already implemented in ECHAM5 is taken into account within the calculation of deposition velocities. Surface resistance for vegetated land surfaces is, among other things a function of leaf resistance, which is directly de-

ECHMERIT model

G. Jung et al.

Full Screen / Esc

pendent on stomata uptake, that is already calculated within ECHAM5, and depends on photosythetically active radiation (PAR) and the available water in the root zone (Sellers et al., 1986). As for land gridcells, aerodynamic, boundary layer and surface resistances are calculated separately and weighted according to the respective frac-
5 tions of water and sea ice/snow, over the ocean area. The grid-average deposition velocities are calculated as the area-weighted average of the deposition velocities for each subgrid fraction. Unlike in the original Wesely approach, no landuse classification is used, as this is not easily derived from ECHAM5. Instead the available landuse dependent values such as LAI, roughness length and stomata resistance are directly
10 transferred from ECHAM5 to the deposition module. The dry deposition scheme is applied to all transported gaseous species.

2.4.2   Particulate dry deposition and sedimentation

With respect to Hg associated with aerosols, ECHMERIT distinguishes between Hg associated with particulate matter that is directly emitted to the atmosphere from an-
15 thropogenic sources, and the Hg associated with particulate matter that is left behind after the evaporation of fog, cloud or rain droplets. The Hg associated with particulate matter which is directly emitted to the atmosphere is considered to be insoluble and is transported as a tracer species until it is either dry deposited or scavenged by cloud droplets and wet deposited. Dry deposition velocities are calculated considering both
20 dry deposition and gravitational settling (sedimentation), according to the approach of Slinn and Slinn (1980), similar to the adaptation within the CAMx regional scale air quality model (CAMx, 2006). Dividing the assumed log-normal particle size distribution into a fixed number of size intervals, the deposition velocity is calculated for each interval and these are subsequently aggregated in a weighted mean. Parameter values
25 for the size distribution, with a geometric mass mean diameter of 0.3 μm and a geometric standard deviation of 1.5 μm were taken from (Pai et al., 1997). The calculation of aerodynamic resistance follows the same approach as for gaseous dry deposition, including the same distinction between types of landcover. Boundary layer resistance

Printer-friendly Version

Interactive Discussion

depends on aerosol Brownian diffusion. Finer surface structures and particle growth in areas of high relative humidity close to the surface, as proposed by Wesely and Hicks (2000) are not considered within this approach.

2.4.3 Wet deposition

An approach of medium complexity was chosen to calculate wet deposition of the transported chemical species. Below-cloud, as well as in-cloud scavenging are considered. This parameterization calculates the loss through wet deposition as proportional to the concentration of air pollutants. The factor of proportionality, that is the scavenging rate, depends on an assumed scavenging efficiency, the total rainfall intensity (gridscale and subgridscale), cloud water content and species solubility according to Henry's law, a mean cloud or rain droplet radius and rain droplet falling velocity, according to the approach of Seinfeld and Pandis (1998), similar to the implementation described in CAMx (2006). No wet deposition is calculated for species with low solubilities (that is with a Henry's law constant of less than $100 \, M \, atm^{-1}$ following Seinfeld and Pandis, 1998). From top to bottom the deposited gaseous species are calculated within each precipitating cell, starting with the first precipitating cloudy layer, which is defined by a cloud water content of at least $0.25 \, g \, m^{-3}$.

Aqueous phase mercury species are considered using a different approach. As well as in transport, also within the deposition routine, all aqueous phase Hg species are treated as one lumped species (Hg_{aq}^{II}). Because these species are already resolved in cloud droplets, the scavenging coefficient approach that is used for the gas-phase species is not applicable here. Assuming a relatively homogeneous distribution of mercury in the cloudy model levels and neglecting the impact that different droplet sizes have on the exchange of species between gas and aqueous phase the following approach was chosen to calculate wet deposition of already scavenged mercury species. Basically the ratio of species mass in aqueous phase and cloud water content is assumed to be equal to the ratio of wet deposited species mass and precipitation. Therefore wet deposition of Hg_{aq}^{II} (d_{wet}) is calculated for each precipitating model column

as

$$d_{\mathrm{wet}} = \frac{\sum_{k=c\mathrm{low}}^{c\mathrm{top}} C_k}{\sum_{k=c\mathrm{low}}^{c\mathrm{top}} W_k} \times P \qquad (5)$$

with $c$low and $c$top, the lowest cloudy and the highest cloudy model layer, C_k the species mass in aqueous phase [kg m^{-2}] and W_k [kg m^{-2}] the cloud water content
5 of a single layer. P is the precipitation of the respective column. This calculation is performed for each column with precipitation over all cloudy model layers below the first precipitating clouds level. Consequently in every cloudy model layer the respective diminuition of C_k, $d_{\mathrm{wet},k}$ is calculated as

$$d_{\mathrm{wet},k} = \frac{C_k}{\sum_{k=c\mathrm{low}}^{c\mathrm{top}} W_k} \times P \qquad (6)$$

10 **2.5 Emissions**

Offline emissions included in the model were derived from the POET emission inventory (Granier et al., 2005). This inventory is an extension of the EDGAR 3 emission dataset (Peters and Olivier, 2003), with an extrapolation of certain precursors over time, and the inclusion of new, satellite based biomass burning data. Furthermore it includes
15 biogenic emissions with adaptations from the GEIA inventories (www.geiacenter.org) and from Mueller and Brasseur (1995). Therein a detailed vegetation canopy model was used for the calculation of isoprene and terpene emissions. These emissions are lumped to species commonly needed in chemical-transport modelling activities.

Anthropogenic mercury emissions were derived form the AMAP emission inventory
20 (Pacyna et al., 2006). These are annual emissions, which means no seasonal cycle is included in anthropogenic mercury emissions. Figure 1 illustrates these emissions, showing clearly the major source regions, that are found in the Northern Hemisphere, in East Asia, Europe and North America, and also in South Africa.

ECHMERIT model

G. Jung et al.

Emissions from forest fires are included in mapping an annual mean value for mercury emissions due to forest fires of $675\,\mathrm{Mg\,y^{-1}}$ (Friedli et al., 2008) to the spatial and temporal distribution of CO biomass burning emissions from the POET emissions inventory (Granier et al., 2005), as illustrated in Fig. 2. Major source regions of forest fire emissions are therefore found in Central and Western Africa, the Amazon region in South America and in Australia. Mercury emissions due to forest fires in the Southern Hemisphere might therefore be a bit overestimated, as the mercury content found in the biosphere is, after all dependent on mercury content in soils and on vegetation cover, which depends on naturally high mercury contents in geologically active zones, as well as on mercury deposited from the atmosphere, which is generally higher in the Northern Hemisphere due to higher mercury concentrations in the atmosphere, following higher anthropogenic emissions.

Ocean emissions are also mapped according to biogenic CO emissions from the ocean, assuming a global annual sum of $3000\,\mathrm{Mg\,y^{-1}}$ of Hg to be emitted from the ocean. A similar approach has been chosen for Hg emissions due to biogenic activities and emissions from soils, with an annual sum of $1669\,\mathrm{Mg\,y^{-1}}$, following Mason (2008). To take into account not only biological activity, but also the dependence of mercury emission from former deposition, two thirds of the emissions from soils and vegetation was mapped according to regions with high deposition rates from a previous model run. The remaining third is solely dependent on vegetational activity and hence mapped with the CO emission from the POET inventory as only one third of natural emissions are assumed to be free from anthropogenic influences. The sum of biogenic emissions and ocean emission is illustrated in Fig. 3. Highest emissions are therefore found from the oceans, and a minimum over desert and polar regions. A more realistic representation of natural emission is required for global mercury modelling, which can be achieved either through sophisticated approaches of online calculation of mercury emissions dependent on soil, biomass and ocean water mercury content – data that is not globally available, or through improved mercury emission inventories, also including natural emissions and their temporal variations.

The data from emission inventories are within a preprocessing step interpolated to the model grid, using the mass conserving remapping tool of the Climate Data Operators (CDO) (Schulzweida et al., 2007) and then serve as input to the simulation and are added to the chemical species concentration within each chemistry time step.

A certain fraction (20%) of wet and dry deposition of RGM, Hg_{aq}^{II} and Hg_p are assumed to be directly re-emitted to the atmosphere as Hg^0 over land areas, an approach similar to the one implemented in the GEOS-chem global mercury simulations (Jaeglé et al., 2008). Re-emissions over the oceans are included within the global annual oceanic emissions and therefore no direct re-emission from the ocean is calculated.

2.6 Model discretization

ECHAM5 is a spectral transform model. The partial differential equations are discretized using a pseudo-spectral method. Vorticity, divergence, temperature and the logarithm of surface pressure are calculated by truncated spherical harmonics, whereas non-linear and diabatic terms, such as moisture and cloud water mixing ratios are calculated on a Gaussian grid. ECHAM5 has a flexible horizontal resolution, and has been applied in resolutions ranging from T21 (5.06 degrees) to T159 (0.75 degrees). For temporal discretization the model uses a semi-implicit leap-frog scheme, and includes a weak time filter to suppress computational modes. In the vertical ECHAM5 is discretized with a hybrid-sigma-pressure system with 19 or 31 non-equidistant layers, with a decreasing model resolution with height. With 19 vertical layers the lower 10–15 layers are tropospheric, the remaining are stratospheric layers. Furthermore a middle atmosphere version of ECHAM5 is available, that has an increased vertical resolution in the mid-atmosphere with 39 to 90 layers up to 0.01 hPa, which was not considered for ECHMERIT so far, as in ECHMERIT only tropospheric chemistry is included.

2.7 Technical implementation

The development of the ECHMERIT model took care that the structure is as modular as possible, to make it flexible and easily applicable for different studies, so that it is possible to include different deposition, emission or chemical schemes without much
5 effort. Like the mixing ratios of water vapour, cloud water etc., the chemical species concentrations are defined in grid-point space and the chemical mechanism is included within the grid-point calculation routine of ECHAM5. The chemical module itself was prepared usind the KPP kinetic preprocessor (Damina-Iordache et al., 2002). Also in the vertical, ECHMERIT uses the same discretization as ECHAM5. Because only tro-
10 pospheric chemistry is included in the model, the calculation of atmospheric chemistry is restricted to the tropospheric model layers. In low resolution model simulations (T42 and lower) the chemistry scheme is called in a smaller time step than the leapfrog-step of the base model, to allow for a more frequent updating of photolysis rates and input of emissions. To avoid negative concentrations that can occur in the case of strong gra-
15 dients, two adaptations of the ECHMA5 transport schemes were implemented. First, the operator splitting (a first oder splitting) was constrained to be strictly sequential for the different processes of transport, deposition, emission and chemistry. Secondly, a mass-conserving flux correction was introduced to the convective tracer mass flux calculation, as described in Sect. 2.2.

20 3 Model setup

For the following examples of model performance and a first evaluation of ECHMERIT the model was run with the setup described below.

Roeckner et al. (2005) showed in a detailed study the sensitivity of the mean climate state simulated by ECHAM5 to horizontal and vertical resolution. Results showed that
25 at a vertical resolution of L19 there is no improvement of model results for horizontal resolutions higher than T42. On the other hand, for T42 horizontal resolution increasing

ECHMERIT model

G. Jung et al.

the number of vertical layers from L19 to L31 did not show any benefit either. As for this first study on model testing and validation, ECHMERIT was run in a T42 resolution, and the L19 vertical resolution was chosen. Of these 19 non-equidistant layers, the upper 4–9 (dependent on latitude) are situated within the stratosphere.

5   Initial and lower boundary SST were taken from the AMIP (Atmospheric Model Inter-comparison Project) (Taylor et al., 1997) reanalysed monthly averaged observational sea surface temperature (SST) data. Land use characteristics, such as roughness length, leaf area index (LAI) and stomata resistance were used directly from ECHAM5. Ozone concentration from the climatology implemented in ECHAM5 was used as

10   the initial concentration and for the stratospheric model layers, where no chemistry is calculated. All other variables are initialized with zero and allowed to spin up until reaching steady-state. A spin-up period of 4 years was necessary to achieve this for mercury.

The simulation period for model evaluation was the year of 2001 and included a

15   nudging of model meteorology to ECMWF ERA40 reanalysis data.

4   Model testing

A complete model validation and statistical analysis is not within the scope of this first model presentation. In the following sections the plausibility of the model results and its general performance is considered, where the major focus lies on surface ozone

20   and mercury concentrations, but deposition calculation is also discussed.

4.1   Deposition velocities

Figures 4, and 5 show examples of the simulated dry deposition velocity of ozone and sulfur dioxide to demonstrate the performance of the dry deposition scheme in ECHMERIT. The influence of solubility (high solubility of SO_2 and low solubility of O_3)

25   can be clearly seen. The ozone dry deposition velocity shows higher values over land

than over the sea, due to its low solubility. For the SO_2 dry deposition velocity the opposite is observed. Very high velocities are observed over the oceans due to the high solubility of SO_2 additionally enhanced in regions with high wind speeds (especially over the Southern oceans). The SO_2 deposition velocities are in good agreement with
5 the simulation results of Ganzeveld et al. (1998). The high solubility and the high reactivity of oxidised mercury leads to a dry deposition velocity for RGM very similar to that of SO_2 (Fig. 6). The ozone dry deposition velocity seems to be overestimated in the antarctic and arctic region over the sea, which can be attributed to the high friction velocities calculated within ECHAM5 over sea ice, which contribute to the calculation
10 of surface and boundary layer resistances. This issue is further investigated.

4.2 O_3 concentrations

Ozone is believed to be one of the major oxidants of elemental mercury (compare Sect. 2.3). Therefore modelling ozone concentrations correctly, in terms of magnitude, and temporal and spatial variability is crucial for the simulation of the oxidation and
15 subsequent removal of mercury from the atmosphere. Hence in a first step of model evaluation, the simulation results for ozone for the year 2001 were analyzed.

In Figs. 7 and 8 the seasonal global distributions of surface ozone for northern hemispheric summer (JJA) and winter (DJF) are illustrated. A clearly seasonally varying ozone concentration with highest values (of up to 80 ppb) over the Mediterranean re-
20 gion and North America in the summer season (JJA) can be observed. Also high values can be observed over the East Asian emission source regions and in central Africa. These high concentrations in Africa during the summer period are caused by ozone precursor emissions in biomass burning plumes during the dry season. Relatively high ozone concentrations are observed in all seasons over the Northern Atlantic
25 and Pacific oceans which is due to the relatively long lifetime of ozone and the transport of precursors away from source regions with the prevailing westerly winds, but also away from enhanced ozone consuming processes/species, that are found in the source regions.

In this context the high values in summer off the North American and Indian coasts are to be highlighted. These are most likely caused by the eastward transport (with the westerlies over the Atlantic and the south-western monsoonal winds over India) of precursor substances. Influenced by source regions in Western India, this can be also ₅ observed in winter over the Indian ocean, when northeasterly winds dominate.

Examples of the comparison between station ozone measurements and the nearest ECHMERIT gridpoint show a reasonable agreement. As demonstrated in the scatter-plot (Fig. 9) ECHMERIT tends to slightly overestimate winter ozone concentrations and underestimate ozone concentrations in summer.

₁₀ Monthly mean ozone concentrations for several stations of the EMEP network are compared in Fig. 10. A good agreement with observations is achieved for mid-latitude stations. Further north the agreement, especially in springtime diminishes. Model results for the stations in the very north of Europe show somewhat poor representation of the annual ozone cycle, where winter concentrations are underestimated. The reasons ₁₅ for this are not entirely clear, but might lie in an underestimation of ozone transport from the stratosphere to the troposphere at that time of the year and in the overestimation of ozone dry deposition velocities over sea ice.

4.3 Hg concentrations

Mercury concentrations are in the following given as volume mixing ration ppqv denom-₂₀ inated briefly as ppq.[1]

An evaluation of model performance for mercury species was achieved considering total gaseous mercury (TGM) in the surface layer and compared to single observational station values of the EMEP observational network (http://tarantula.nilu.no/projects/ccc/emepdata.html). Figure 11 illustrates the annual mean surface TGM con-₂₅ centration [ppq], as simulated by ECHMERIT. Higher mercury concentrations in the

---

[1]For an approximate comparison to the more commonly used measure of $ng\,m^{-3}$: at standard atmospheric surface layer conditions (20°C and 1013.25 hPa) $1\,ng\,m^{-3} = 119.4\,ppq$.

Northern Hemisphere can be delineated, especially near source regions in Europe, North America and East Asia, where values of over 300 ppq are reached. According to observations (Lindberg et al., 2007), the gradient between Northern and Southern Hemisphere is more pronounced than in this ECHMERIT simulation. This can be at-
5 tributed to the relatively high emissions of mercury from the oceans, that make up more than half of the global annual emissions of mercury. These emissions, if mapped with the CO emissions from the POET emission inventory, as currently is the case in ECHMERIT, somewhat overestimate mercury emissions from the southern oceans especially during the Southern Hemisphere summer, due to the strong link between
10 CO emissions and biological activity and because the spatial distributions of previously deposited mercury is neglected. Additionally, possibly the atmospheric lifetime of Hg in the Southern Hemisphere is smaller due to a higher concentration of bromine follow-ing a higher sea-salt aerosol production in the Southern Hemisphere caused by higher wind speeds (Yang et al., 2005).
15   The scatterplot (Fig. 12), showing monthly mean TGM concentrations of all available EMEP stations compared to the modelled values at the nearest grid point demonstrate a reasonable model performance. Apart from the summer months (JJA) TGM concen-tration tends to be underestimated in the simulation. This is, as mentioned before due to the overestimation of mercury emissions from the oceans, from soil, vegetation and
20 biomass burning in the Southern Hemisphere, which consequently means an underes-timation of mercury emission in the Northern Hemisphere, because the global annual emission sums are restricted to the predefined values, but the distribution depends ba-sically on the one derived from CO emission inventories (compare Sect. 2.5). Therefore the background concentrations in the Northern Hemisphere are underestimated during
25 autumn/winter.

4.4 Statistical measures for mercury and ozone validation

In Table 5 some statistical measures for ozone as well as mercury are summarized. A description is given in Table 4. Most of the measures are based on Chang and Hanna

(2004). These are calculated from observational data from the EMEP network and the respective nearest gridpoints of the simulation. The mean bias (MB) and geometric mean bias (MG) are both measures to capture systematic biases of the model. These are both comparably small, but MG is a little larger for mercury (13.55 ppq). Also summarized are the mean gross error (MAGE) and the normalized MAGE (MNGE) [%] (that is normalized according to the observational mean value). The MNGE indicates a relatively smaller deviation for the mercury concentrations (11%) than for ozone (33%). This is most likely influenced by the generally higher variability of ozone that is harder to reproduce, than the variability of mercury species which is relatively smaller with respect to the background concentrations. In contrast to MG, the geometric variance (VG) shows the relative scatter, which is composed of systematic, as well as random errors. These values also show satisfying results for both O_3 (1.23) and TGM (1.02). Generally a satisfactory model performance is obtained from these statistical analysis of model results with respect to observation data. Nevertheless, it has to be pointed out that comparing only observational point data to the simulation values, which are representative of the mean concentrations in the entire grid cell cannot give a precise look at model performance, therefore model validation has to be extended in future studies.

4.5 Mercury deposition processes

Before wet deposition of mercury species can be evaluated it is reasonable to evaluate model performance with respect to precipitation. In Tost et al. (2006) a comparison of different convective parameterizations within the ECHAM5/MESSy modelling system was performed. Model resolution was T42 with 31 vertical layers, and therefore the obtained results cannot be completely comparable to our study, as the vertical resolution has a strong impact on strength and position of the Hadley cell and on the location of the mid-latitude westerlies as illustrated for ECHAM5 by Roeckner et al. (2005). Nevertheless the study of Tost et al. (2006) demonstrated large differences in precipitation fields due to differences in convective parameterizations, whereas simu-

lated water vapour columns were similar and matched observations very well. Annual mean precipitation was overestimated with all convection schemes over the continents in the tropics and in the southern storm tracks.

Figure 13 demonstrates the annual simulated precipitation for the year 2001 of the ECHMERIT run. Annual wet deposition of TGM is illustrated in Fig. 14. An obvious dependence on precipitation pattern is found, but additionally the deposition amount depends on the emission strength in source regions, which can be seen for the Southern Pacific and Indian ocean, but also for the strong sources in East Asia. Of this wet deposited mercury, 87.6% is below-cloud scavenged RGM, whereas 12.36% is Hg[II](aq) that rained out and was already present in cloud droplets, taking part in aqueous-phase chemistry. Wet deposition maxima over the US are found over the eastern parts of the country which is in agreement with measurements and a modelling study of Selin et al. (2007).

Dry deposition (Fig. 15) in this model simulation is 99.43% RGM. Due to the very low deposition velocities for elemental mercury this is negligible. Major dry deposition of mercury therefore not only occurs near source regions, but also a pronounced amount of deposited mercury is found for the tropics, where the largest quantity of oxidised mercury is found, following the O_3 and OH distribution, as well as the higher temperatures, that favour oxidation reactions of elemental mercury with these two oxidants. Inline with other modelling studies (Seigneur et al., 2004; Selin et al., 2007; Hedgecock et al., 2006) the larger fraction of deposition over Europe and North America is due to dry deposition.

5 Performance on a multiple-processor linux cluster

The performance of the coupled modelling system was tested on a Red-Hat Linux cluster with up to 20 (XEON, 3.06 GHz) processors. Figure 16 shows the performance of the model, illustrating ratios of wallclock times, for different model setups and as a function of the number of processors.

First the model performance for a different number of processors was analysed (Fig. 16, top), and shows a strong decrease of computing time with respect to a one-processor run especially for up to 12 cpus.

Another performance test was performed for the different chemical schemes. First a simulation with only gas phase chemistry was run. The relative increase in simulation time for different runs, including, aqueous, as well as dry chemistry is then demonstrated in Fig. 16 (middle). Here WET indicated the gas+aqueous phase chemistry scheme with the calculation of the transfer coefficient from the gas phase to cloud droplets assuming a mean droplet radius. The simulations FL2 to FL1000 represent simulations in which the calculation of the averaged mass transfer coefficient was performed dividing the droplet size distribution function into a number of bins from 2 to 1000. This shows that generally, a large increase in computational time can be expected with an increase in the number of droplet bins used in the calculation. A significant difference in model results, with respect to the number of bins into which the size distribution was divided could only be detected when the number of bins was less than 2 in box model experiments.

The computational time required to run ECHMERIT for a given period with 20 cpus is about 6% of the time required using 1 cpu. In contrast, running ECHMERIT without chemistry included (which is very near to a pure ECHAM5 simulation) on 20 cpus requires approximately 20% (Fig. 16 bottom) of the time for the run on one cpu only. ECHMERIT (with chemistry) requires almost 20 times as long to perform a simulation for a given period when compared to the original ECHAM5 (no chemistry).

6 Conclusions and outlook

The new global mercury-chemistry and transport model ECHMERIT has undergone an initial performance evaluation and a detailed description of all important developed model components was given. These included a precise description of the modules for wet and dry deposition calculation, the implemented emission databases, as well

Back | Close

Full Screen / Esc

Printer-friendly Version

Interactive Discussion

as the chemistry scheme used to simulate tropospheric photochemistry and mercury chemistry. The ECHMERIT model aims to minimize modelling inconsistencies, that are a common problem in CTMs. As ECHMERIT is run in online coupled mode, meteorology, emissions, deposition and chemistry are calculated contemporaneously and on the same model grid. Therefore modelling uncertainties due to interpolation of meteorological input variables on the CTM model grid and also uncertainties due to the lack of representation of high-frequency meteorology features are reduced. ECHMERIT also uses the same convective transport scheme for model physics as for tracer transport. Not doing this can lead to additional inconsistencies, as in common offline coupled models. A first model evaluation demonstrated a satisfying model performance for ozone and mercury compounds. Some immediately identified problems lie in the inadequate representation of mercury emissions from oceans, vegetation, soils and biomass burning, as these compounds were entirely or partly derived from a mapping of CO emissions to reported annual mercury emissions. This neglects the fact, that a large amount of so-called natural emissions (from oceans, soils and biosphere) are in fact formerly deposited mercury compounds of anthropogenic origin. Therefore one major task in ongoing model development must be the implementation of improved emission inventories for non-anthropogenic emissions or the development of sophisticated routines for online calculation of natural emissions, for which global soil, ocean and biomass Hg concentration distributions are necessary. This has a high potential to improve the representation of the assumed hemispheric mercury gradient and the seasonal cycle of mercury concentrations in both hemispheres. As outlined before, also the inclusion of a bromine climatology and an activation of bromine chemistry in ECHMERIT might improve the north-south gradient significantly, because from that a stronger mercury depletion over the Southern Hemisphere oceans is expected.

Nevertheless, anthropogenic emissions also have a major uncertainty, because the anthropogenic emission data bases currently available, and used within all global models neglect the temporal variation of mercury emissions. Additionally model improvements could be achieved by introducing volcanic mercury emissions, as well as light-

ning NO_x emissions for photochemistry.

Ongoing work includes a precise model validation and statistical analysis for a larger range of tropospheric chemistry variables and based on a larger variety of observational data (surface data, soundings, aircraft measurements, ship cruises etc.). To

5 achieve this task, especially for mercury species an intensification of measurements is important, as one of the main problems regarding model validation lies in the very small amount of observational data available for mercury compounds. Especially, there is a large gap considering almost the entire Southern Hemisphere and oceanic areas and there is also a lack of upper air data and vertical profiles.

10 Notwithstanding the uncertainties mentioned above, ECHMERIT is suitable for the simulation of mercury chemistry, transport and deposition fluxes on a global scale. ECHMERIT includes state-of-the-art process descriptions of all important processes (emissions, deposition, transport and chemistry) and is characterized by a modular structure and therefore a high level of flexibility that also allows extended sensitivity

15 testing for different chemistry schemes. This is especially useful, because of the uncertainty regarding the tropospheric reactions of mercury and its compounds in the gas and aqueous phases.

Global scale models are useful both for the investigation of intercontinental transport and global scale characteristics of concentration, emission and deposition fields and

20 for the provision of spatio-temporally varying boundary conditions for more detailed regional models. The former is important due to the abject lack of available measurement data from which to infer or extrapolate to from point measurements to area estimates of Hg loadings for example. In the latter case, it has been amply demonstrated by Pongprueksa et al. (2007) that fixed boundary condition concentrations are inappropriate for

25 regional models. In fact they found that the model response to a change in the Hg^0 concentration boundary condition was almost linear. Global models therefore serve both to identify large scale transport phenomena and synoptic scale source-receptor relationships but also to improve the performance of more detailed, more highly spatially resolved regional models.

Appendix A

Chemistry mechanisms

See Tables A1 and A2.

References

Ariya, P. A., Khalizov, A., and Gidas, A.: Reactions of gaseous mercury with atomic and molecular halogens: kinetics, product studies, and atmospheric implications, J. Phys. Chem. A, 106, 7310–7320, 2002. 424

Ariya, P. A., Snider, G., and Amyot, M.: Mercury transformation at environmental surfaces: Feedbacks to the atmosphere, chapter 15, in: Mercury Fate and Transport in the Global Atmosphere: Measurements, Models and Policy Implications; Interim Report of the UNEP Global Partnership on Atmospheric Mercury Transport and Fate Research, 345–376, 2008. 396, 397

Atkinson, R., Baulch, D. L., Cox, R. A., Crowley, J. N., Hampson, R. F., Hynes, R. G., Jenkin, M. E., Rossi, M. J., Troe, J., and IUPAC Subcommittee: Evaluated kinetic and photochemical data for atmospheric chemistry: Volume II – gas phase reactions of organic species, Atmos. Chem. Phys., 6, 3625–4055, 2006, http://www.atmos-chem-phys.net/6/3625/2006/. 428

Bey, I., Jacob, D. J., Yantosca, R. M., Logan, J. A., Field, B. D., Fiore, A. M., Li, Q., Liu, H. Y., Mickley, L. J., and Schultz, M. G.: Global modeling of tropospheric chemistry with assimilated meteorology – Model description and evaluation, J. Geophys. Res., 106, 23073–23095, 2001. 389

Brinkop, S. and Sausen, R.: A finite difference approximation for convective transports which

Printer-friendly Version

Interactive Discussion

maintains positive tracer concentrations, Contributions to Atmospheric Physics, 70, 245–248, 1997. 394

Bullock, O. R.: Current methods and research strategies for modeling atmospheric mercury, Fuel Process. Technol., 65–66, 459–471, 2000. 387

5 CAMx: CAMx, user's guide, version 4.40, Environ International Corporation, California, 2006. 399, 400

Chang, J. C. and Hanna, S. R.: Air quality model performance evaluation, Meteorol. Atmos. Phys., 87, 167–196, 2004. 408

Christensen, J. H., Brandt, J., Frohn, L. M., and Skov, H.: Modelling of Mercury in the Arctic
10 with the Danish Eulerian Hemispheric Model, Atmos. Chem. Phys., 4, 2251–2257, 2004, http://www.atmos-chem-phys.net/4/2251/2004/. 389

Clever, H. L., Johnson, S. A., and Derrick, M. E.: The solubility of Mercury and Some Sparingly Soluble Mercury Salts in Water and Aqueous Electrolyte Solutions, J. Phys. Chem. Ref. Data, 14, 631–680, 1985. 425

15 Damina-Iordache, V., Sandu, A., Damian-Iordache, M., Carmichael, G. R., and Potra, F. A.: The kinetic preprocessor KPP: a software environment for solving chemical kinetics, Computers Chemical Engineering, 26, 1567–1579, 2002. 394, 404

Dastoor, A. P. and Larocque, Y.: Global circulation of atmospheric mercury: a modelling study, Atmos. Environ., 38, 147–161, 2004. 390

20 Ebinghaus, R., Kock, H. H., Coggins, A. M., Spain, T. G., Jennings, S. G., and Temme, C.: Long-term measurements of atmospheric mercury at Mace Head, Irish west coast, between 1995 and 2001, Atmos. Environ., 36, 5267–5276, 2002. 388

Ebinghaus, R., Banic, C., Beauchamp, S., Jaffe, D., Kock, H. H., Pirrone, N., Poissant, L., Sprovieri, F., and Weiss, P. S.: Spatial coverage and temporal trends of land-based atmo-
25 spheric mercury measurements in the northern and southern hemispheres, chapter 9, in: Mercury Fate and Transport in the Global Atmosphere: Measurements, Models and Policy Implications; Interim Report of the UNEP Global Partnership on Atmospheric Mercury Transport and Fate Research, 168–219, 2008. 388

Eckhardt, S., Stohl, A., Beirle, S., Spichtinger, N., James, P., Forster, C., Junker, C., Wagner, T.,
30 Platt, U., and Jennings, S. G.: The North Atlantic Oscillation controls air pollution transport to the Arctic, Atmos. Chem. Phys., 3, 1769–1778, 2003, http://www.atmos-chem-phys.net/3/1769/2003/. 386

Friedli, H. R., Arellano, A. F., Cinnirella, S., and Pirrone, N.: Mercury emissions from global

ECHMERIT model

G. Jung et al.

Title Page

Abstract	Introduction
Conclusions	References
Tables	Figures

◄◄   ►►

◄   ►

Back   Close

Full Screen / Esc

Printer-friendly Version

Interactive Discussion

biomass burning: spatial and temporal distribution, chapter 8, in: Mercury Fate and Transport in the Global Atmosphere: Measurements, Models and Policy Implications; Interim Report of the UNEP Global Partnership on Atmospheric Mercury Transport and Fate Research, 145–167, 2008. 402

5 Ganzeveld, L. and Lelieveld, J.: Dry deposition parameterization in a chemistry-general circulation model and its influence on the distribution of reactive trace gases, J. Geophys. Res., 100, 20999–21012, 1995. 398

Ganzeveld, L., Lelieveld, J., and Roelofs, G.-J.: A dry deposition parameterization for sulfur oxides in a chemistry and general circulation model, J. Geophys. Res., 103, 5679–5694,
10 1998. 398, 406

Ganzeveld, L. N., van Aardenne, J. A., Butler, T. M., Lawrence, M. G., Metzger, S. M., Stier, P., Zimmermann, P., and Lelieveld, J.: Technical Note: Anthropogenic and natural offline emissions and the online EMissions and dry DEPosition submodel EMDEP of the Modular Earth Submodel system (MESSy), Atmos. Chem. Phys. Discuss., 6, 5457–5483, 2006,
15 http://www.atmos-chem-phys-discuss.net/6/5457/2006/. 398

Gårdfeldt, K. and Jonsson, M.: Is bimolecular reduction of Hg(II) complexes possible in aqueous systems of environmental importance, J. Phys. Chem. A, 107, 4478–4482, 2003. 397, 425

Granier, C., Lamarque, J. F., Mieville, A., Muller, J. F., Olivier, J., Orlando, J., Peters, J., Petron,
20 G., Tyndall, G., and Wallens, S.: POET, a database of surface emissions of ozone precursors, available at: http://www.aero.jussieu.fr/projet/ACCENT/POET.php, 2005. 401, 402

Hagemann, S.: An improved land surface parameter dataset for global and regional climate models, Max-Planck-Institut für Meteorologie, 2002. 392

Hall, B.: The gas phase oxidation of elemental mercury by ozone, Water Air Soil Poll., 80,
25 301–315, 1995. 396, 397, 424

Hall, B. and Bloom, N. S.: Report to the Electric Power Research Institute, Palo Alto, CA, 1993. 424

Hedgecock, I. M. and Pirrone, N.: Chasing quicksilver: Modeling the atmospheric lifetime of $Hg^0(g)$ in the marine boundary layer at various latitudes, Environ. Sci. Technol., 38, 69–76,
30 2004. 388

Hedgecock, I. M., Trunfio, G. A., Pirrone, N., and Sprovieri, F.: Mercury chemistry in the MBL: Mediterranean case and sensitivity studies using the AMCOTS (Atmospheric Mercury Chemistry over the Sea) model, Atmos. Environ., 39, 7217–7230, doi:10.1016/j.atmosenv.2005.09.

ECHMERIT model

G. Jung et al.

⏮ | ⏭

◀ | ▶

Back | Close

Full Screen / Esc

Printer-friendly Version

Interactive Discussion

002, 2005. 396

Hedgecock, I. M., Pirrone, N., Trunfio, G. A., and Sprovieri, F.: Integrated mercury cycling, transport, and air-water exchange (MECAWEx) model, J. Geophys. Res., 111, D20302, doi: 10.1029/2006JD007117, 2006. 410

5 Horowitz, L. W., Walters, S., Mauzerall, D. L., Emmons, L. K., Rasch, P. J., Granier, C., Tie, X., Lamarque, J. F., Schultz, M. G., Tyndall, G. S., et al.: A global simulation of tropospheric ozone and related tracers: Description and evaluation of MOZART, version 2, J. Geophys. Res., 108(D24), 4784, doi:10.1029/2002JD002853, 2003. 390

Hynes, A. J., Donohoue, D. L., Goodsite, M. E., and Hedgecock, I. M.: Our current understand-
10 ing of major chemical and physical processes affecting mercury dynamics in the atmosphere and at the air-water/terrestrial interfaces, chapter 14, in: Mercury Fate and Transport in the Global Atmosphere: Measurements, Models and Policy Implications Interim Report of the UNEP Global Partnership on Atmospheric Mercury Transport and Fate Research, 322–344, 2008. 396, 397

15 Jacobson, M. Z.: Fundamentals of Atmospheric Modeling, Cambridge University Press, 1999. 398

Jaeglé, L., Strode, S. A., Selin, N. E., and Jacob, D. J.: The GEOS-chem model, chapter 18, in: Mercury Fate and Transport in the Global Atmosphere: Measurements, Models and Policy Implications; Interim Report of the UNEP Global Partnership on Atmospheric Mercury
20 Transport and Fate Research, 401–410, 2008. 403

Kerkweg, A., Buchholz, J., Ganzeveld, L., Pozzer, A., Tost, H., and Jöckel, P.: Technical Note: An implementation of the dry removal processes DRY DEPosition and SEDImentation in the Modular Earth Submodel System (MESSy), Atmos. Chem. Phys., 6, 4617–4632, 2006, http://www.atmos-chem-phys.net/6/4617/2006/. 398

25 Liang, Q., Jaeglé, L., Jaffe, D. A., Weiss-Penzias, P., Heckman, A., and Snow, J. A.: Long-range transport of Asian pollution to the northeast Pacific: Seasonal variations and transport pathways of carbon monoxide, J. Geophys. Res., 109, D23S07, doi:10.1029/2003JD004402, 2004. 386

Lin, C.-J. and Pehkonen, S. O.: Aqueous free radical chemistry of mercury in the presence of
30 iron oxides and ambient aerosol, Atmos. Environ., 31, 4125–4137, 1997. 425

Lin, C.-J. and Pehkonen, S. O.: Aqueous Phase Reactions of Mercury with Free Radicals and Chlorine: Implications for Atmospheric Mercury Chemistry, Chemosphere, 38, 1253–1263, 1999. 425

ECHMERIT model

G. Jung et al.

⏮ | ⏭

◀ | ▶

Back | Close

Full Screen / Esc

Printer-friendly Version

Interactive Discussion

Lin, S. J. and Rood, R. B.: Multidimensional Flux-Form Semi-Lagrangian Transport Schemes, Mon. Weather Rev., 124, 2046–2070, 1996. 392

Lindberg, S., Bullock, R., Ebinghaus, R., Engstrom, D., Feng, X., Fitzgerald, W., Pirrone, N., Prestbo, E., and Seigneur, C.: A synthesis of progress and uncertainties in attributing the sources of mercury in deposition, AMBIO: A Journal of the Human Environment, 36, 19–33, 2007. 386, 388, 408

Lohman, K., Seigneur, C., Gustin, M., and Lindeberg, S.: Sensitivity of the global atmospheric cycle of mercury to emissions, Appl. Geochem., 23, 454–466, doi:10.1016/j.apgeochem. 2007.12.022, 2008. 390

Lott, F. and Miller, M.: The Representation of Sub-Grid Scale Orography in GCMs, NATO ASI SERIES I, Global Environ. Chang., 50, 275–290, 1997. 392

Lubick, N.: Ocean mercury on the increase, Nature, published online, doi:10.1038/news.2009. 218, 2009. 387

Mason, R. P.: Mercury emissions from natural sources and their importance in the global mercury cycle, chapter 7, in: Mercury Fate and Transport in the Global Atmosphere: Measurements, Models and Policy Implications; Interim Report of the UNEP Global Partnership on Atmospheric Mercury Transport and Fate Research, 130–144, 2008. 402

Mueller, J.-F. and Brasseur, G.: IMAGES: a three-dimensional chemical transport model of the global troposphere, J. Geophys. Res., 100, 16445–16490, 1995. 401

Munthe, J.: The aqueous oxidation of elemental mercury by ozone, Atmos. Environ., 26A, 1461–1468, 1992. 425

Nordeng, T. E.: Extended Versions of the Convective Parametrization Scheme at ECMWF and Their Impact on the Mean and Transient Activity of the Model in the Tropics, European Centre for Medium-Range Weather Forecasts, 1994. 392

Pacyna, E. G., Pacyna, J. M., Steenhuisen, F., and Wilson, S.: Global anthropogenic mercury emission inventory for 2000, Atmos. Environ., 40, 4048–4063, 2006. 387, 401

Pacyna, J. M., Pacyna, E. G., and Aas, W.: Changes of emissions and atmospheric deposition of mercury, lead, and cadmium, Atmos. Environ. International, 43, 117–127, 2009. 389

Pai, P., Karamchandani, P., and Seigneur, C.: Simulation of the regional atmospheric transport and fate of mercury using a comprehensive Eulerian model, Atmos. Environ., 31, 2717–2732, 1997. 399

Pal, B. and Ariya, P. A.: Studies of ozone initiated reactions of gaseous mercury: kinetics, product studies, and atmospheric implications, Phys. Chem. Chem. Phys., 6, 572–579, 2004.

Full Screen / Esc

Printer-friendly Version

Interactive Discussion

396, 424

Pehkonen, S. O. and Lin, C.-J.: Aqueous photochemistry of mercury with organic acids, JAPCA J. Air Waste Ma. (1995), 48, 144–150, 1998. 397, 425

Peters, J. A. H. W. and Olivier, J. G. J.: EDGAR3/POET Enussuibs; 1997 emissions and sce-
narios for 1995–2020; Technical background infromation on global and regional sectoral emissions, RIVM, Bilthoven, report no. 773301003, 2003. 401

Pirrone, N. and Mason, R.: Mercury Fate and Transport in the Global Atmosphere: Measure-
ments, Models and Policy Implications Interim Report of the UNEP Global Partnership on Atmospheric Mercury Transport and Fate Research, 2008. 387

Pirrone, N. and Mason, R. (Eds.): Mercury Fate and Transport in the Global Atmosphere: Emissions, Measurements and Models, Springer, USA, 2009. 387

Pirrone, N., Keeler, G. J., and Nriagu, J. O.: Regional differences in worldwide emissions of mercury to the atmosphere, Atmos. Environ., 17, 2981–2987, 1996. 387

Pleijel, K. and Munthe, J.: Modelling the Atmospheric Mercury Cycle – Chemistry in Fog Droplets, Atmos. Environ., 29, 1441–1457, 1995. 425

Pongprueksa, P., Lin, C. J., Lindberg, S. E., Jang, C., Braverman, T., Russell Bullock, O., Ho, T. C., and Chu, H. W.: Scientific uncertainties in atmospheric mercury models III: Bound-
ary and initial conditions, model grid resolution, and Hg (II) reduction mechanism, Atmos. Environ., 42, 1828–1845, 2007. 397, 413

Roeckner, E., Baeuml, G., Bonventura, L., Brokopf, R., Esch, M., Giorgetta, M., Hagemann, S., Kirchner, I., Kornblueh, L., Manzini, E., Rhodin, A., Schlese, U., Schulzweida, U., and Tomp-
kins, A.: The atmospheric general circulation model ECHAM5. PART I: Model description, Report 349, Max Planck Institute for Meteorology, Hamburg, Germany, 2003. 391

Roeckner, E., Brokopf, R., Esch, M., Giorgetta, M., Hagemann, S., Kornblueh, L., Manzini, E., Schlese, U., and Schulzweida, U.: Sensitivity of Simulated Climate to Horizontal and Vertical Resolution in the ECHAM5 Atmosphere Model, J. Climate, 19, 3771–3791, 2005. 391, 404, 409

Sander, R.: Modeling Atmosheric Chemistry: Interactions between Gas-Phase Species and Liquid Cloud/Aerosol Particles, Survey of Geophysics, 20, 1–31, 1999. 395

Sander, R., Kerkweg, A., Jöckel, P., and Lelieveld, J.: Technical note: The new comprehensive atmospheric chemistry module MECCA, Atmos. Chem. Phys., 5, 445–450, 2005, http://www.atmos-chem-phys.net/5/445/2005/. 395, 434

Sander, S. P., Friedl, R. R., Golden, D. M., Kurylo, M. J., Moortgat, G. K., Keller-Rudek, H.,

Wine, P. H., Ravishankara, A. R., Kolb, C. E., Molina, M. J., Finlayson-Pitts, B. J., Huie, R. E., and Orkin, V. L.: Chemical kinetics and photochemical data for use in atmospheric studies evaluation number 15, National Aeronautics and Space Administration, Jet Propulsion Laboratory, California Institute of Technology, 2006. 428

5   Sandu, A. and Sander, R.: Technical note: Simulating chemical systems in Fortran90 and Matlab with the Kinetic PreProcessor KPP-2.1, Atmos. Chem. Phys., 6, 187–195, 2006, http://www.atmos-chem-phys.net/6/187/2006/. 397

Schroeder, W. H., Anlauf, K.-G., Barrie, L. A., Lu, J. Y., Steffen, A., Schneeberger, D. R., and Berg, T.: Arctic springtime depletion of mercury, Nature, 394, 331–332, 1998. 387, 425

10 Schulzweida, U., Kornblueh, L., and Quast, R.: CDO User's Guede, Climate Data Operators, Version 1.0.7, Tech. rep., www.mpimet.mpg.de/fileadmin/software/cdo/, 2007. 403

Schwartz, S. E.: Mass-transport considerations pertinent to aqueous phase reactions of gases in liquid-water clouds, in: Chemistry of Multiphase Atmospheric Systems NATO ASI Series G6, edited by: Jaeschle, W., Springer Berlin Heidelberg, Germany, 415–471, 1986. 395

15 Seigneur, C., Lohman, K., Vijayaraghavan, K., and Shia, R.-L.: Multiscale modeling of the atmospheric fate and transport of mercury, J. Geophys. Res., 106(D21), 27795–27809, 2001. 390

Seigneur, C., Karamchandani, P., Vijayaraghavan, K., Lohman, K., Shia, R. L., and Levin, L.: On the effect of spatial resolution on atmospheric mercury modeling, Sci. Total Environ., 304,
20 73–81, 2003. 390

Seigneur, C., Vijayaraghavan, K., Lohmann, K., Karamchandani, P., and Scott, C.: Global source attribution for mercury deposition in the United States, Environ. Sci. Technol., 38, 555–569, 2004. 390, 410

Seigneur, C., Vijayaraghavan, K., and Lohman, K.: Atmospheric mercury chemistry: Sensitivity
25 of global model simulations to chemical reactions, J. Geophys. Res., 111, D22306, doi: 10.1029/2005JD006780, 2006. 390

Seinfeld, C. P. and Pandis, S. N.: Atmospheric Chemistry and Physics, From Air Pollution to Climate Change, John Wiley and Sons Inc, ISBN 0-4 71-17816-0, 1998. 400

Selin, N. E., Jacob, D. J., Park, R. J., Yantosca, R. M., Strode, S., Jaeglé, L., and Jaffe, D.:
30 Chemical cycling and deposition of atmospheric mercury: Global constraints from observations, J. Geophys. Res., 112, D02308, doi:10.1029/2006JD007450, 2007. 410

Sellers, P. J., Mintz, Y., Sud, Y. C., and Dalcher, A.: A simple biosphere model (SiB) for use within general circulation models, Journal of Atmospheric Sciences, 43, 505–531, 1986. 399

ECHMERIT model

G. Jung et al.

Title Page

Abstract | Introduction

Conclusions | References

Tables | Figures

◄ | ►

◄ | ►

Back | Close

Full Screen / Esc

Printer-friendly Version

Interactive Discussion

Slemr, F. and Scheel, H. E.: Trends in atmospheric mercury concentrations at the summit of the Wank mountain, Southern Germany, Atmos. Environ., 32, 845–853, 1998. 388

Slemr, F., Brunke, E. G., Ebinghaus, R., Temme, C., Munthe, J., Wängberg, I., Schroeder, W., Steffen, A., and Berg, T.: Worldwide trend of atmospheric mercury since 1977, Geophys. Res. Lett., 30, 1516, doi:10.1029/2003GL016954, 2003. 388

Slinn, S. A. and Slinn, W. G. N.: Prediction for particle deposition of natural waters, Atmos. Environ., 14, 1013–1016, 1980. 399

Sommar, J., Hallquist, M., Ljungström, E., and Lindqvist, O.: On the gas phase reactions between volatile biogenic mercury species and the nitrate radical, J. Atmos. Chem., 27, 233–247, 1997. 424

Sommar, J., Gårdfeldt, K., Strömberg, D., and Feng, X.: A kinetic study of the gas-phase reaction between the hydroxyl radical and atomic mercury, Atmos. Environ., 35, 3049–3054, 2001. 424

Sprovieri, F., Pirrone, N., Hedgecock, I. M., Landis, M. S., and Stevens, R. K.: Intensive atmospheric mercury measurements at Terra Nova Bay in Antarctica during November and December 2000, J. Geophys. Res., 107(D23), 4722, doi:10.1029/2002JD002057, 2002. 387

Stohl, A., Eckhardt, S., Forster, C., James, P., and Spichtinger, N.: On the pathways and timescales of intercontinental air pollution transport, J. Geophys. Res, 107(D23), 4684, doi:10.1029/2001JD001396, 2002. 386

Taylor, K. E., Williamson, D., and Zwiers, F.: AMIPII Sea Surface Temperature and Sea Ice Concentration Boundary Conditions, 1997. 405

Tiedtke, M.: A Comprehensive Mass Flux Scheme for Cumulus Parameterization in Large-Scale Models, Mon. Weather Rev., 117, 1779–1800, 1989. 392

Tokos, J. J. S., Hall, B., Calhoun, J. A., and Prestbo, E. M.: Homogeneous gas-phase reaction of Hg^0 with H_2O_2, O_3, CH_3I, and $(CH_3)_2S$: Implications for atmospheric Hg cycling, Atmos. Environ. (1994), 32, 823–827, 1998. 424

Tost, H., Jöckel, P., and Lelieveld, J.: Influence of different convection parameterisations in a GCM, Atmos. Chem. Phys., 6, 5475–5493, 2006, http://www.atmos-chem-phys.net/6/5475/2006/. 409

Travnikov, O.: Contribution of the intercontinental atmospheric transport to mercury pollution in the Northern Hemisphere, Atmos. Environ., 39, 7541–7548, 2005. 389

Van Loon, L. L., Mader, E. A., and Scott, S. L.: Sulfite Stabilization and Reduction of the Aqueous Mercuric Ion: Kinetic Determination of Sequential Formation Constants, J. Phys.

Printer-friendly Version

Interactive Discussion

Chem. A, 105, 3190–3195, 2001. 425

Vijayaraghavan, K., Karamchandani, P., Seigneur, C., Balmori, R., and Chen, S. Y.: Plume-in-grid modeling of atmospheric mercury, J. Geophys. Res.-Atmos., 113, D24305, doi:10.1029/2008JD010580, 2008. 397

5 Wang, Z. and Pehkonen, S. O.: Oxidation of elemental mercury by aqueous bromine: atmospheric implications, Atmos. Environ., 38, 3675–3688, 2004. 425

Wesely, M. L.: Parameterization of the surface resistances to gaseous dry deposition in regional-scale numerical models, Atmos. Environ., 23, 1293–1304, 1989. 398

Wesely, M. L. and Hicks, B. B.: Some factors that affect the deposition rates of sulfur dioxide
10 and similar gases on vegetation, Journal of Air Pollution Control Assessment, 27, 1110–1116, 1977. 398

Wesely, M. L. and Hicks, B. B.: A review of the current status of knowledge on dry deposition, Atmos. Environ., 34, 2261–2282, 2000. 400

Wild, O., Zhu, X., and Prather, M. J.: Fast-J: Accurate Simulation of In-and Below-Cloud Pho-
15 tolysis in Tropospheric Chemical Models, J. Atmos. Chem., 37, 245–282, 2000. 395

Yang, X., Cox, R., Warwick, N., Pyle, J., Carver, G., O'Connor, F., and Savage, N.: Tropospheric bromine chemistry and its impacts on ozone: A model study, J. Geophys. Res.-Atmos., 110, D23311, doi:10.1029/2005JD006244, 2005. 408

Zaveri, R. A. and Peters, L. K.: A new lumped structure photochemical mechanism for large-
20 scale applications, J. Geophys. Res., 104, 30387–30415, 1999. 395, 428

Table 1. Transported chemical species in ECHMERIT.

	Chemical Species
CO	carbon monoxide
Hg	gaseous elemental mercury
HgO	oxidised mercury
O_3	ozone
NH_3	ammonia
ANOL	ethanole and higher alcohols
$HgCl_2$	mercury dichloride
C_2H_6	ethane
TOL	toluene
XYL	xylene
CH_3OH	methanol
SO_2	sulfur dioxide
ETH	ethene
PAR	paraffin carbon
OLET	terminal olefin carbons
AONE	acetone
OLEI	internal olefin carbons
ISOP	isoprene
ALD2	acetaldehyde
HCHO	formaldehyde
HNO_3	nitric acid
NO	nitric oxide
NO_2	nitrogen dioxide
Hg_p	particulate mercury
$Hg^{II}(aq)$	lumped divalent acqueous phase Hg

Table 2. Gas phase mercury chemistry reactions and equilibria included in ECHMERIT, following (a) Hall (1995), (b) Pal and Ariya (2004), (c) Tokos et al. (1998), (d) Sommar et al. (2001), (e) Hall and Bloom (1993), (f) Ariya et al. (2002), (g) Sommar et al. (1997).

Reaction	k or K (298 K)	Reference
$Hg^0 + O_3 \rightarrow HgO$	$3.0 \times 10^{-20} \, cm^3 \, molec^{-1} \, s^{-1}$	(a)
$Hg^0 + O_3 \rightarrow HgO$	$7.5 \times 10^{-19} \, cm^3 \, molec^{-1} \, s^{-1}$	(b)
$Hg^0 + H_2O_2 \rightarrow HgO$	$8.5 \times 10^{-19} \, cm^3 \, molec^{-1} \, s^{-1}$	(c)
$Hg^0 + OH \rightarrow HgO$	$8.7 \times 10^{-14} \, cm^3 \, molec^{-1} \, s^{-1}$	(d)
$Hg^0 + HCl \rightarrow\rightarrow HgCl_2$	$1 \times 10^{-19} \, cm^3 \, molec^{-1} \, s^{-1}$	(e)
$Hg^0 + Br \rightarrow HgBr$	$3.2 \times 10^{-12} \, cm^3 \, molec^{-1} \, s^{-1}$	(f)
$Hg^0 + NO_3 \rightarrow HgO + NO_2$	$4.0 \times 10^{-15} \, cm^3 \, molec^{-1} \, s^{-1}$	(g)

ECHMERIT model

G. Jung et al.

Table 3. Aqueous phase mercury chemistry reactions and equilibria included in ECHMERIT.

Reaction	k or K (298 K)	Reference
$Hg^0(aq) + O_3(aq) \rightarrow HgO(aq)$	$4.7 \times 10^7\,M^{-1}\,s^{-1}$	Munthe (1992)
$HgO(aq) + H^+(aq) \rightarrow Hg^{++}(aq) + OH^-(aq)$	$1 \times 10^{10}\,M^{-1}\,s^{-1}$	Pleijel and Munthe (1995)
$Hg^{++}(aq) + OH^-(aq) \rightarrow HgOH^+(aq)$	$3.9 \times 10^{10}\,M^{-1}$	Pleijel and Munthe (1995)
$HgOH^+(aq) + OH^-(aq) \rightarrow Hg(OH)_2(aq)$	$1.6 \times 10^{11}\,M^{-1}$	Pleijel and Munthe (1995)
$HgOH^+(aq) + Cl^-(aq) \rightarrow HgOHCl(aq)$	$2.7 \times 10^7\,M^{-1}$	Pleijel and Munthe (1995)
$Hg^{++}(aq) + Cl^-(aq) \rightarrow HgCl^+(aq)$	$5.8 \times 10^6\,M^{-1}$	Pleijel and Munthe (1995)
$HgCl^+(aq) + Cl^-(aq) \rightarrow HgCl_2(aq)$	$2.5 \times 10^6\,M^{-1}$	Pleijel and Munthe (1995)
$Hg^{++}(aq) + Br^-(aq) \rightarrow HgBr^+(aq)$	$1.1 \times 10^9\,M^{-1}$	Clever et al. (1985)
$HgBr^+(aq) + Br^-(aq) \rightarrow HgBr_2(aq)$	$2.5 \times 10^8\,M^{-1}$	Clever et al. (1985)
$Hg^{++}(aq) + SO_3^{--}(aq) \rightarrow HgSO_3(aq)$	$2.1 \times 10^{13}\,M^{-1}$	Van Loon et al. (2001)
$HgSO_3(aq) + SO_3^{--}(aq) \rightarrow Hg(SO_3)_2^{--}(aq)$	$1.0 \times 10^{10}\,M^{-1}$	Van Loon et al. (2001)
$HgSO_3(aq) \rightarrow Hg^0(aq) + products$	$T\exp((31.971 \times T) - 12595)/T\,s^{-1}$	Van Loon et al. (2001)
$Hg^0(aq) + OH(aq) \rightarrow Hg^+(aq) + OH^-(aq)$	$2.0 \times 10^9\,M^{-1}\,s^{-1}$	Lin and Pehkonen (1997)
$Hg^+(aq) + OH(aq) \rightarrow Hg^{++}(aq) + OH^-(aq)$	$1.0 \times 10^{10}\,M^{-1}\,s^{-1}$	Lin and Pehkonen (1997)
$Hg^{II}(aq) + O_2^-(aq) \rightarrow Hg^+(aq) + O_2(aq)$	$1.1 \times 10^4\,M^{-1}\,s^{-1}$	Pehkonen and Lin (1998)
$Hg^{II}(aq) + HO_2(aq) \rightarrow Hg^+(aq) + O_2(aq) + H^+(aq)$	$1.1 \times 10^4\,M^{-1}\,s^{-1}$	Pehkonen and Lin (1998)
$Hg^I(aq) + O_2^-(aq) \rightarrow Hg(aq) + O_2(aq)$	fast	Pehkonen and Lin (1998)
$Hg^I(aq) + HO_2(aq) \rightarrow Hg^0(aq) + O_2(aq) + H^+(aq)$	fast	Pehkonen and Lin (1998)
$Hg^{II}(aq) + O_2^-(aq) \rightarrow Hg^+(aq) + O_2(aq)$	0	Gårdfeldt and Jonsson (2003)
$Hg^{II}(aq) + HO_2(aq) \rightarrow Hg^+(aq) + O_2(aq) + H^+(aq)$	0	Gårdfeldt and Jonsson (2003)
$Hg(aq) + HOCl(aq) \rightarrow Hg^{++}(aq) + Cl^-(aq) + OH^-(aq)$	$2.09 \times 10^6\,M^{-1}\,s^{-1}$	Lin and Pehkonen (1999)
$Hg(aq) + ClO^-(aq) \rightarrow Hg^{++}(aq) + Cl^-(aq) + OH^-(aq)$	$1.99 \times 10^6\,M^{-1}\,s^{-1}$	Lin and Pehkonen (1999)
$Hg(aq) + HOBr(aq) \rightarrow Hg^{++}(aq) + Br^-(aq) + OH^-(aq)$	$0.279\,M^{-1}\,s^{-1}$	Wang and Pehkonen (2004)
$Hg(aq) + OBr^-(aq) \rightarrow Hg^{++}(aq) + Br^-(aq) + OH^-(aq)$	$0.273\,M^{-1}\,s^{-1}$	Wang and Pehkonen (2004)
$Hg(aq) + Br_2(aq) \rightarrow Hg^{++}(aq) + 2Br^-(aq) + OH^-(aq)$	$0.196\,M^{-1}\,s^{-1}$	Wang and Pehkonen (2004)
$Hg^0(g) \leftrightarrow Hg^0(aq)$	$0.13\,M\,atm^{-1}$	Schroeder et al. (1998)
$HgO(g) \leftrightarrow HgO(aq)$	$2.69 \times 10^{12}\,M\,atm^{-1}$	Schroeder et al. (1998)
$HgCl_2(g) \leftrightarrow HgCl_2(aq)$	$2.75 \times 10^6\,M\,atm^{-1}$	Schroeder et al. (1998)
$HgBr_2(g) \leftrightarrow HgBr_2(aq)$	$2.75 \times 10^6\,M\,atm^{-1}$	Schroeder et al. (1998)

Printer-friendly Version

Interactive Discussion

Table 4. Statistical measures of model performance with M_i modelled value and O_i observed value.

name	variable	equation
geometric mean bias	MG	$\exp(\overline{lnO} - \overline{lnM})$
mean bias	MB	$\frac{1}{N} \sum_{i=1}^{N} (M_i - O_i)$
mean absolute gross error	MAGE	$\frac{1}{N} \sum_{i=1}^{N} |M_i - O_i|$
mean normalized gross error	MNGE	$\frac{1}{N} \sum_{i=1}^{N} \frac{|M_i - O_i|}{O_i} \times 100$
geometric variance	VG	$\exp[(lnO - lnM)^2]$

ECHMERIT model

G. Jung et al.

Full Screen / Esc

Table 5. Statistical measures for ozone and mercury modelling results evaluation.

	Ozone	TGM
modelled mean	30.40 ppb	161.83 ppq
measured mean	31.86 ppb	175.38 ppq
modelled max	76.34 ppb	187.57 ppq
measured max	66.37 ppb	213.04 ppq
modelled min	5.19 ppb	134.03 ppq
measured min	7.47 ppb	134.82 ppq
MG	1.14	1.08
MB	1.46 ppb	13.55 ppq
MAGE	9.72 ppb	20.22 ppq
MNGE	32.53%	11.22%
VG	1.23	1.02

Table A1. Gas phase chemistry reactions and equilibria included in ECHMERIT, rate constants according to: (ph) – photolysis rate constant calculated online; (1) – CBM-Z (Zaveri and Peters, 1999); (2) – Sander et al. (2006); (3) – Atkinson et al. (2006).

Reaction	Reference
$NO_2 + hv \rightarrow NO + O(^3P)$	(ph)
$NO_3 + hv \rightarrow NO + O_2$	(ph)
$NO_3 + hv \rightarrow NO_2 + O_3P$	(ph)
$HONO + hv \rightarrow OH + NO$	(ph)
$HNO_3 + hv \rightarrow OH + NO_2$	(ph)
$HNO_4 + hv \rightarrow HO_2 + NO_2$	(ph)
$N_2O_5 + hv \rightarrow NO_2 + NO_3$	(ph)
$O_3 + hv \rightarrow O(^3P)$	(ph)
$O_3 + hv \rightarrow O(^1D)$	(ph)
$H_2O_2 + hv \rightarrow 2OH$	(ph)
$O^1(D) + O_2 \rightarrow O(^3P) + O_2$	(2)
$O^1(D) + N_2 \rightarrow O(^3P) + N_2$	(2)
$O^1(D) + H_2O \rightarrow 2OH$	(2)
$O(^3P) + O_2 \rightarrow O_3$	(1)
$O(^3P) + O_3 \rightarrow 2O_2$	(1)
$O(^3P) + NO_2 \rightarrow NO + O_2$	(2)
$O(^3P) + NO_2 \rightarrow NO_3$	(2)
$O(^3P) + NO \rightarrow NO_2$	(1)
$O_3 + NO \rightarrow NO_2 + O_2$	(2)
$O_3 + NO_2 \rightarrow NO_3 + O_2$	(1)
$O_3 + OH \rightarrow HO_2 + O_2$	(2)
$O_3 + HO_2 \rightarrow OH + 2O_2$	(2)
$OH + H_2 \rightarrow HO_2$	(2)
$OH + NO \rightarrow HONO$	(1)
$OH + NO_2 \rightarrow HNO_3$	(2)
$OH + NO_3 \rightarrow HO_2 + NO_2$	(1)

ECHMERIT model

G. Jung et al.

Title Page

Abstract | Introduction

Conclusions | References

Tables | Figures

|◄ | ►|

◄ | ►

Back | Close

Full Screen / Esc

Printer-friendly Version

Interactive Discussion

Table A1. Continued.

Reaction	Reference
$OH + HONO \rightarrow NO_2$	(1)
$OH + HNO_3 \rightarrow NO_3$	(2)
$OH + HNO_4 \rightarrow NO_2$	(1)
$OH + HO_2 \rightarrow H_2O + O_2$	(1)
$OH + H_2O_2 \rightarrow HO_2$	(2)
$HO_2 + HO_2 \rightarrow H_2O_2$	(2)
$HO_2 + HO_2 + H_2O \rightarrow H_2O_2$	(2)
$HO_2 + NO \rightarrow OH + NO_2$	(1)
$HO_2 + NO_2 \rightarrow HNO_4$	(2)
$HO_2 + NO_2 \rightarrow HONO$	(1)
$HNO_4 \rightarrow HO_2 + NO_2$	(2)
$NO_3 + NO \rightarrow NO_2 + NO_2$	(1)
$NO_3 + NO_2 \rightarrow NO + NO_2$	(1)
$NO_3 + NO_2 \rightarrow N_2O_5$	(2)
$NO_3 + NO_3 \rightarrow NO_2 + NO_2$	(1)
$NO_3 + HO_2 \rightarrow 0.3HNO_3 + 0.7NO_2 + 0.7OH$	(1)
$N_2O_5 + H_2O \rightarrow HNO_3 + HNO_3$	(1)
$N_2O_5 \rightarrow NO_3 + NO_2$	(2)
$CO + OH \rightarrow HO_2$	(2)
$SO_2 + OH \rightarrow H_2SO_4 + HO_2$	(1)
$CH_4 + OH \rightarrow CH_3O_2$	(1)
$C_2H_6 + OH \rightarrow ETHP$	(1)
$CH_3OH + OH \rightarrow HCHO + HO_2$	(2)
$HCHO + hv \rightarrow 2HO_2 + CO$	(ph)
$HCHO + hv \rightarrow CO$	(ph)
$HCHO + OH \rightarrow HO_2 + CO$	(2)
$HCHO + NO_3 \rightarrow HNO_3 + HO_2 + CO$	(2)

Table A1. Continued.

Reaction	Reference
$CH_3OOH + hv \rightarrow HCHO + HO_2 + OH$	(ph)
$ETHOOH + hv \rightarrow ALD2 + HO_2 + OH$	(ph)
$CH_3OOH + OH \rightarrow 0.7CH_3O_2 + 0.3HCHO + 0.3OH$	(1)
$ETHOOH + OH \rightarrow 0.5ETHP + 0.5ALD2 + 0.5OH$	(1)
$CH_3O_2 + NO \rightarrow HCHO + HO_2 + NO_2$	(2)
$ETHP + NO \rightarrow ALD2 + HO_2 + NO_2$	(1)
$CH_3O_2 + NO_3 \rightarrow HCHO + HO_2 + NO_2$	(3)
$ETHP + NO_3 \rightarrow ALD2 + HO_2 + NO_2$	(3)
$CH_3O_2 + HO_2 \rightarrow CH_3OOH$	(2)
$ETHP + HO_2 \rightarrow ETHOOH$	(1)
$CH_3O_2 \rightarrow 0.66HCHO + 0.32HO_2 + 0.34CH_3OH$	(1)
$ETHP \rightarrow 0.8ALD2 + 0.6HO_2 + 0.2C_2H_6$	(1)
$ANOL + OH \rightarrow ALD2 + HO_2$	(1)
$ALD2 + hv \rightarrow CH_3O_2 + HO_2 + CO$	(ph)
$ALD2 + OH \rightarrow C_2O_3$	(1)
$ALD2 + NO_3 \rightarrow C_2O_3 + HNO_3$	(1)
$C_2O_3 + NO_2 \rightarrow PAN$	(1)
$PAN \rightarrow C_2O_3 + NO_2$	(1)
$C_2O_3 + NO \rightarrow NO_2 + CH_3O_2$	(2)
$C_2O_3 + NO_3 \rightarrow NO_2 + CH_3O_2$	(1)
$C_2O_3 + HO_2 \rightarrow 0.4RCOOH + 0.4O_3$	(1)
$C_2O_3 \rightarrow CH_3O_2$	(1)
$PAR + OH \rightarrow RO_2$	(1)
$AONE + hv \rightarrow C_2O_3 + CH_3O_2$	(ph)
$AONE + OH \rightarrow ANO2$	(2)
$MGLY + hv \rightarrow C_2O_3 + CO + HO_2$	(ph)

ECHMERIT model

G. Jung et al.

Table A1. Continued.

Reaction	Reference
$MGLY + OH \rightarrow XO_2 + C_2O_3$	(1)
$MGLY + NO_3 \rightarrow HNO_3 + C_2O_3 + CO$	(1)
$ETH + O_3 \rightarrow HCHO + 0.22HO_2 + 0.12OH + 0.24CO + 0.52HCOOH$	(1)
$ETH + OH \rightarrow XO_2 + 1.56HCHO + HO_2 + 0.22ALD2$	(3)
$OLET + O_3 \rightarrow 0.57HCHO + 0.47ALD2 + 0.33OH + 0.26HO_2 + 0.07CH_3O_2 + 0.06ETHP + 0.03RO_2 + 0.13C_2O_3 + 0.04MGLY + 0.03CH_3OH + 0.31CO + 0.22HCOOH + 0.09RCOOH + 1.06XPAR$	(1)
$OLEI + O_3 \rightarrow 0.07AONE + 1.03ALD2 + 0.6OH + 0.22HO_2 + 0.1CH_3O_2 + 0.05ETHP + 0.09RO_2 + 0.11ANO2 + 0.19C_2O_3 + 0.07MGLY + 0.04CH_3OH + 0.3CO + 0.16RCOOH + 2.26XPAR$	(1)
$OLET + OH \rightarrow XO_2 + HO_2 + HCHO + ALD2 + XPAR$	(1)
$OLEI + OH \rightarrow XO_2 + HO_2 + 0.23AONE + 1.77ALD2 + 2.23XPAR$	(1)
$OLET + NO_3 \rightarrow NAP$	(1)
$OLEI + NO_3 \rightarrow NAP$	(1)
$TOL + OH \rightarrow 0.08XO_2 + 0.12CRES + 0.2HO_2 + 0.8TO_2$	(1)
$XYL + OH \rightarrow 0.5XO_2 + 0.55HO_2 + 0.05CRES + 0.8MGLY + 1.1PAR + 0.45TO_2$	(1)
$TO_2 + NO \rightarrow 0.95NO_2 + 0.95OPEN + 0.95HO_2 + 0.05ONIT$	(1)
$CRES + OH \rightarrow 0.4CRO + 0.6XO_2 + 0.6HO_2 + 0.3OPEN$	(1)
$CRES + NO_3 \rightarrow CRO + HNO_3$	(1)
$CRO + NO_2 \rightarrow ONIT$	(1)
$OPEN + OH \rightarrow XO_2 + C_2O_3 + 2CO + 2HO_2 + HCHO$	(1)
$OPEN + hv \rightarrow C_2O_3 + CO + HO_2$	(ph)
$OPEN + O_3 \rightarrow 0.03ALD2 + 0.62C_2O_3 + 0.7HCHO + 0.69CO + 0.08OH + 0.03XO_2 + 0.76HO_2 + 0.2MGLY$	(1)

Table A1. Continued.

Reaction	Reference
ROOH + hv → OH + 0.4XO$_2$ + 0.74AONE + 0.3ALD2+ 0.1ETHP + 0.9HO$_2$ + 1.98XPAR	(ph)
ROOH + OH → 0.77RO$_2$ + 0.19MGLY + 0.04ALD2 + 0.23OH+ 0.42XPAR	(1)
ONIT + OH → NAP	(1)
ONIT + hv → NO$_2$ + 0.41XO$_2$ + 0.74AONE + 0.3ALD2+ 0.1ETHP + 0.9HO$_2$ + 1.98XPAR	(ph)
RO$_2$ + NO → 0.16ONIT + 0.84NO$_2$ + 0.34XO$_2$ + 0.62AONE+ 0.25ALD2 + 0.08ETHP + 0.76HO$_2$ + 1.68XPAR	(1)
ANO2 + NO → NO$_2$ + C$_2$O$_3$ + HCHO	(1)
NAP + NO → 1.5NO$_2$ + 0.5HCHO + 0.5ALD2 + 0.5ONIT+ 0.5HO$_2$ + XPAR	(1)
XO$_2$ + NO → NO$_2$	(1)
RO$_2$ + NO$_3$ → NO$_2$ + 0.4XO$_2$ + 0.74AONE + 0.3ALD2+ 0.1ETHP + 0.9HO$_2$ + 1.98XPAR	(1)
ANO2 + NO$_3$ → NO$_2$ + C2O3 + HCHO	(1)
NAP + NO$_3$ → 1.5NO$_2$ + 0.5HCHO + 0.5ALD2 + 0.5ONIT+ 0.5HO$_2$ + XPAR	(1)
XO$_2$ + NO$_3$ → NO$_2$	(1)
RO$_2$ + HO$_2$ → ROOH	(1)
ANO2 + HO$_2$ → ROOH	(1)
NAP + HO$_2$ → ONIT	(1)
XO$_2$ + HO$_2$ → PROD	(1)
RO$_2$ → 0.24XO$_2$ + 0.21ALD2 + 0.57AONE + 0.06ETHP+ 0.54HO$_2$ + 1.25XPAR	(1)
ANO2 → 0.7C$_2$O$_3$ + 0.7HCHO + 0.15MGLY + 0.15AONE	(1)
NAP → 0.5NO$_2$ + 0.5HCHO + 0.5ALD2 + 0.5ONIT + XPAR	(1)
XO$_2$ → PROD	(1)

Printer-friendly Version

Interactive Discussion

Table A1. Continued.

Reaction	Reference
PAR + XPAR → PROD	(1)
ISOP + OH → ISOPP + 0.08XO$_2$	(1)
ISOP + O$_3$ → 0.6HCHO + 0.65ISOPRD + 0.27OH + 0.07HO$_2$+ 0.07CO + 0.39HCOOH + 0.15ALD2 + 0.2XO$_2$ + 0.2C$_2$O$_3$	(1)
ISOP + NO$_3$ → ISOPN	(1)
ISOPRD + hv → 0.97C$_2$O$_3$ + 0.33HO$_2$ + 0.33CO + 0.7CH$_3$O$_2$+ 0.2HCHO + 0.07ALD2 + 0.03AONE	(ph)
ISOPRD + OH → 0.5C$_2$O$_3$ + 0.5ISOPO$_2$ + 0.2XO$_2$	(1)
ISOPRD + O$_3$ → 0.27OH + 0.1HO$_2$ + 0.11C$_2$O$_3$ + 0.07XO$_2$+ 0.05CH$_3$O$_2$ + 0.16CO + 0.15HCHO + 0.02ALD2 + 0.09AONE+ 0.85MGLY + 0.46RCOOH	(1)
ISOPRD + NO$_3$ → 0.07C$_2$O$_3$ + 0.07HNO$_3$ + 0.64CO+ 0.28HCHO + 0.93ONIT + 0.28ALD2 + 0.93HO$_2$ + 0.93XO$_2$+ 1.86PAR	(1)
ISOPP + NO → 0.09ONIT + 0.91NO$_2$ + 0.91HO$_2$ + 0.63HCHO+ 0.91ISOPRD + 0.18PAR	(1)
ISOPN + NO → 1.2NO$_2$ + 0.8ONIT + 0.8ALD2 + 0.8HO$_2$+ 0.2ISOPRD + 1.6PAR	(1)
ISOPO$_2$ + NO → NO$_2$ + HO$_2$ + 0.59CO + 0.55ALD2+ 0.25HCHO + 0.34MGLY + 0.63AONE	(1)
ISOPP + HO$_2$ → ROOH	(1)
ISOPN + HO$_2$ → ONIT + 2PAR	(1)
ISOPO$_2$ + HO$_2$ → ROOH	(1)
ISOPP → ISOPRD	(1)
ISOPN → ALD2 + ONIT + 2PAR	(1)
ISOPO$_2$ → 0.5ALD2 + 0.5AONE	(1)

Table A2. Aqueous phase chemistry reactions and equilibria included in ECHMERIT as from the MECCA model (Sander et al., 2005).

Reaction
$HO_2(aq) \rightarrow H^+(aq) + O_2^-(aq)$
$H^+(aq) + O_2^-(aq) \rightarrow HO_2(aq)$
$H_2O(aq) \rightarrow H^+(aq) + OH^-(aq)$
$H^+(aq) + OH^-(aq) \rightarrow H_2O(aq)$
$NH_4^+(aq) \rightarrow NH_3(aq) + H^+(aq)$
$NH_3(aq) + H^+(aq) \rightarrow NH_4^+(aq)$
$HONO(aq) \rightarrow H^+(aq) + NO_2^-(aq)$
$H^+(aq) + NO_2^-(aq) \rightarrow HONO(aq)$
$HNO_3(aq) \rightarrow H^+(aq) + NO_3^-(aq)$
$H^+(aq) + NO_3^-(aq) \rightarrow HNO_3(aq)$
$HNO_4(aq) \rightarrow H^+(aq) + NO_4^-(aq)$
$H^+(aq) + NO_4^-(aq) \rightarrow HNO_4(aq)$
$CO_2(aq) \rightarrow H^+(aq) + HCO_3^-(aq)$
$H^+(aq) + HCO_3^-(aq) \rightarrow CO_2(aq)$
$HCOOH(aq) \rightarrow H^+(aq) + HCOO^-(aq)$
$H^+(aq) + HCOO^-(aq) \rightarrow HCOOH(aq)$
$HSO_3^-(aq) \rightarrow H^+(aq) + SO_3^{--}(aq)$
$H^+(aq) + SO_3^{--}(aq) \rightarrow HSO_3^-(aq)$
$H_2SO_4(aq) \rightarrow H^+(aq) + HSO_4^-(aq)$
$H^+(aq) + HSO_4^-(aq) \rightarrow H_2SO_4(aq)$
$HSO_4^-(aq) \rightarrow H^+(aq) + SO_4^{--}(aq)$
$H^+(aq) + SO_4^{--}(aq) \rightarrow HSO_4^-(aq)$
$SO_2(aq) \rightarrow H^+(aq) + HSO_3^-(aq)$
$H^+(aq) + HSO_3^-(aq) \rightarrow SO_2(aq)$
$HCl(aq) \rightarrow H^+(aq) + Cl^-(aq)$
$H^+(aq) + Cl^-(aq) \rightarrow HCl(aq)$

ECHMERIT model

G. Jung et al.

Table A2. Continued.

Reaction
$O_3(aq) + O_2^-(aq) \rightarrow OH(aq) + O_2(aq) + O_2(aq) + OH^-(aq)$
$OH(aq) + OH(aq) \rightarrow H_2O_2(aq)$
$HO_2(aq) + O_2^-(aq) \rightarrow H_2O_2(aq) + O_2(aq) + OH^-(aq)$
$OH(aq) + HO_2(aq) \rightarrow H_2O(aq) + O_2(aq)$
$HO_2(aq) + HO_2(aq) \rightarrow H_2O_2(aq) + O_2(aq)$
$OH(aq) + H_2O_2(aq) \rightarrow H_2O(aq) + HO_2(aq)$
$NO_2^-(aq) + O_3(aq) \rightarrow NO_3^-(aq)$
$NO_2(aq) + NO_2(aq) \rightarrow HONO(aq) + HNO_3(aq)$
$NO_4^-(aq) \rightarrow NO_2^-(aq)$
$HO_2(aq) + NO_2(aq) \rightarrow HNO_4(aq)$
$NO_2^-(aq) + OH(aq) \rightarrow NO_2(aq) + OH^-(aq)$
$NO_3(aq) + OH^-(aq) \rightarrow NO_3^-(aq) + OH(aq)$
$HONO(aq) + OH(aq) \rightarrow NO_2(aq)$
$HONO(aq) + H_2O_2(aq) + H^+(aq) \rightarrow NO_3^-(aq)$
$CO_3^-(aq) + O_2^-(aq) \rightarrow HCO_3^-(aq) + OH^-(aq)$
$CO_3^-(aq) + H_2O_2(aq) \rightarrow HO_2(aq) + HCO_3^-(aq)$
$CO_3^-(aq) + HCOO^-(aq) \rightarrow HCO_3^-(aq) + HCO_3^-(aq) + HO_2(aq)$
$HCOO^-(aq) + OH(aq) \rightarrow OH^-(aq) + HO_2(aq) + CO_2(aq)$
$HCO_3^-(aq) + OH(aq) \rightarrow CO_3^-(aq)$
$HCHO(aq) + OH(aq) \rightarrow HCOOH(aq) + HO_2(aq)$
$HCOOH(aq) + OH(aq) \rightarrow HO_2(aq) + CO_2(aq)$
$CH3OO(aq) + O_2^-(aq) \rightarrow CH_3OOH(aq) + OH^-(aq)$
$CH_3OO(aq) + HO_2(aq) \rightarrow CH_3OOH(aq)$
$CH_3OH(aq) + OH(aq) \rightarrow HCHO(aq) + HO_2(aq)$
$CH_3OOH(aq) + OH(aq) \rightarrow CH_3OO(aq)$
$CH_3OOH(aq) + OH(aq) \rightarrow HCHO(aq) + OH(aq)$
$SO_3^-(aq) + O_2(aq) \rightarrow SO_5^-(aq)$

Table A2. Continued.

Reaction
$SO_3^{--}(aq) + O_3(aq) \rightarrow SO_4^{--}(aq)$
$SO_4^-(aq) + O_2^-(aq) \rightarrow SO_4^{--}(aq)$
$SO_4^-(aq) + SO_3^{--}(aq) \rightarrow SO_3^{--}(aq) + SO_4^{--}(aq)$
$SO_5^-(aq) + O_2^-(aq) \rightarrow HSO_5^-(aq) + OH^-(aq)$
$SO_5^-(aq) + SO_3^{--}(aq) \rightarrow 0.28SO_3^-(aq) + 0.28HSO_5^-(aq) + 0.72SO_4^-(aq) +$
$0.72SO_4^{--}(aq) + 0.28OH^-(aq)$
$SO_5^-(aq) + SO_5^-(aq) \rightarrow O_2(aq)$
$SO_3^{--}(aq) + OH(aq) \rightarrow SO_3^-(aq) + OH^-(aq)$
$SO_4^{--}(aq) + OH(aq) \rightarrow HSO_5^-(aq)$
$SO_4^-(aq) + HO_2(aq) \rightarrow SO_4^{--}(aq) + H^+(aq)$
$SO_4^-(aq) + H_2O(aq) \rightarrow SO_4^{--}(aq) + H^+(aq) + OH(aq)$
$SO_4^-(aq) + H_2O_2(aq) \rightarrow SO_4^{--}(aq) + H^+(aq) + HO_2(aq)$
$HSO_3^-(aq) + O_2^-(aq) \rightarrow SO_4^{--}(aq) + OH(aq)$
$HSO_3^-(aq) + O_3(aq) \rightarrow SO_4^{--}(aq) + H^-(aq)$
$HSO_3^-(aq) + OH(aq) \rightarrow SO_3^-(aq) + H_2O(aq)$
$HSO_3^-(aq) + HO_2(aq) \rightarrow SO_4^{--}(aq) + H^+(aq) + OH(aq)$
$HSO_3^-(aq) + H_2O_2(aq) \rightarrow SO4^{--}(aq) + H^+(aq)$
$HSO_3^-(aq) + SO_4^-(aq) \rightarrow SO_3^-(aq) + SO_4^{--}(aq) + H^+(aq)$
$HSO_3^-(aq) + SO_5^-(aq) \rightarrow 0.75SO_4^-(aq) + 0.75SO_4^-(aq) + 0.75H^+(aq) +$
$0.25SO_3^-(aq) + 0.25HSO_5^-(aq)$
$HSO_3^-(aq) + HSO_5^-(aq) + H^+(aq) \rightarrow 2SO_4^{--}(aq) + 2H^+(aq)$
$SO_3^{--}(aq) + NO_2(aq) \rightarrow SO_4^{--}(aq) + 2HONO(aq) - NO_2(aq)$
$SO_4^-(aq) + NO_3^-(aq) \rightarrow SO_4^{--}(aq) + NO_3(aq)$
$SO_4^{--}(aq) + NO_3(aq) \rightarrow NO_3^-(aq) + SO_4^-(aq)$
$HSO_3^-(aq) + NO_2(aq) \rightarrow HSO_4^-(aq) + 2HONO(aq) - NO_2(aq)$
$HSO_3^-(aq) + NO_3(aq) \rightarrow SO_3^-(aq) + NO_3^-(aq) + H^+(aq)$
$HSO_3^-(aq) + HNO_4(aq) \rightarrow HSO_4^-(aq) + NO_3^-(aq) + H^+(aq)$

Table A2. Continued.

Reaction
$SO_3^{--}(aq) + HCHO(aq) \rightarrow CH_2OHSO_3^-(aq)$
$SO_3^{--}(aq) + CH_3OOH(aq) + H^+(aq) \rightarrow SO_4^{--}(aq) + H^+(aq) + CH_3OH(aq)$
$HSO_3^-(aq) + HCHO(aq) \rightarrow CH_2OHSO_3^-(aq)$
$HSO_3^-(aq) + CH_3OOH(aq) + H^+(aq) \rightarrow SO_4^{--}(aq) + H^+(aq) + H^+(aq) +$
$CH_3OH(aq)$
$CH_2OHSO_3^-(aq) + OH^-(aq) \rightarrow SO_3^{--}(aq) + HCHO(aq)$
$O_3(aq) + h\nu \rightarrow OH(aq) + OH(aq) + O_2(aq)$
$H_2O_2(aq) + h\nu \rightarrow OH(aq) + OH(aq)$
$O_3(aq) \rightarrow O_3$
$O_2(aq) \rightarrow O_2$
$OH(aq) \rightarrow OH$
$HO_2(aq) \rightarrow HO_2$
$H_2O_2(aq) \rightarrow H_2O_2$
$NH_3(aq) \rightarrow NH_3$
$CH_3OO(aq) \rightarrow CH_3O_2$
$CH_3OOH(aq) \rightarrow CH_3OOH$
$HCHO(aq) \rightarrow HCHO$
$HCOOH(aq) \rightarrow HCOOH$
$HCl(aq) \rightarrow HCl$
$CO_2(aq) \rightarrow CO_2$
$SO_2(aq) \rightarrow SO_2$
$NO_2(aq) \rightarrow NO_2$
$NO_3(aq) \rightarrow NO_3$
$HONO(aq) \rightarrow HONO$
$HNO_3(aq) \rightarrow HNO_3$
$H_2SO_4 \rightarrow SO_4^{--}(aq) + H^+(aq) + H^+(aq)$
$N_2O_5 + H_2O(aq) \rightarrow HNO_3(aq) + HNO_3(aq)$
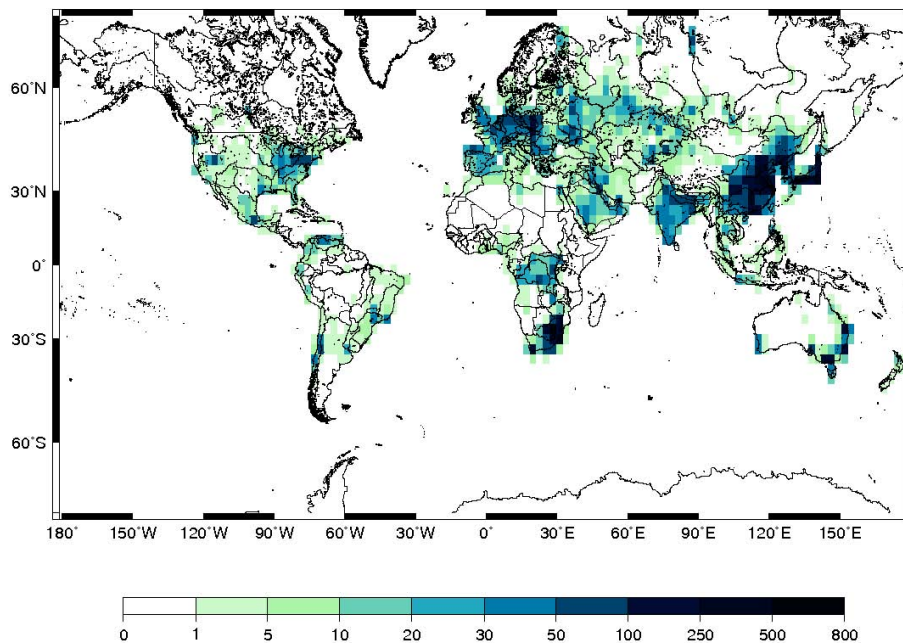
Fig. 1. Annual anthropogenic TGM emissions [kg m^{-2}].
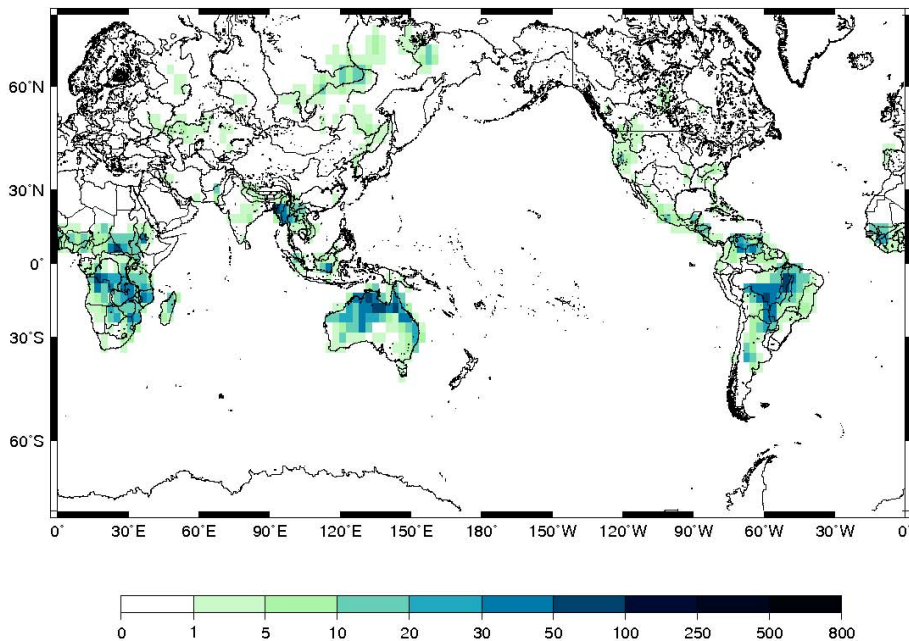
Fig. 2. Annual biomass burning elemental Hg emissions [$kg\,m^{-2}$].
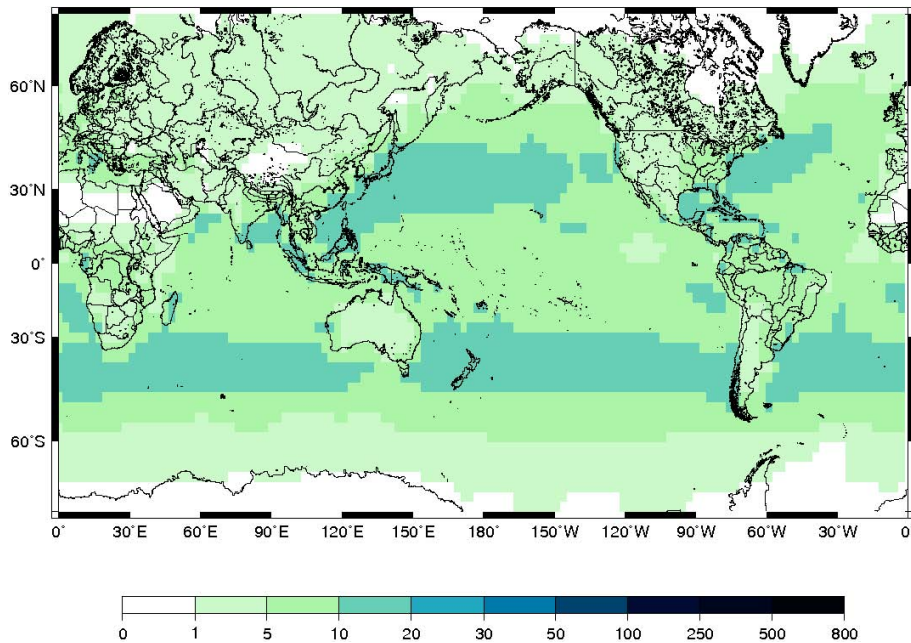
Fig. 3. Annual natural (ocean and vegetation/soil) elemental Hg emissions $[\text{kg m}^{-2}]$.
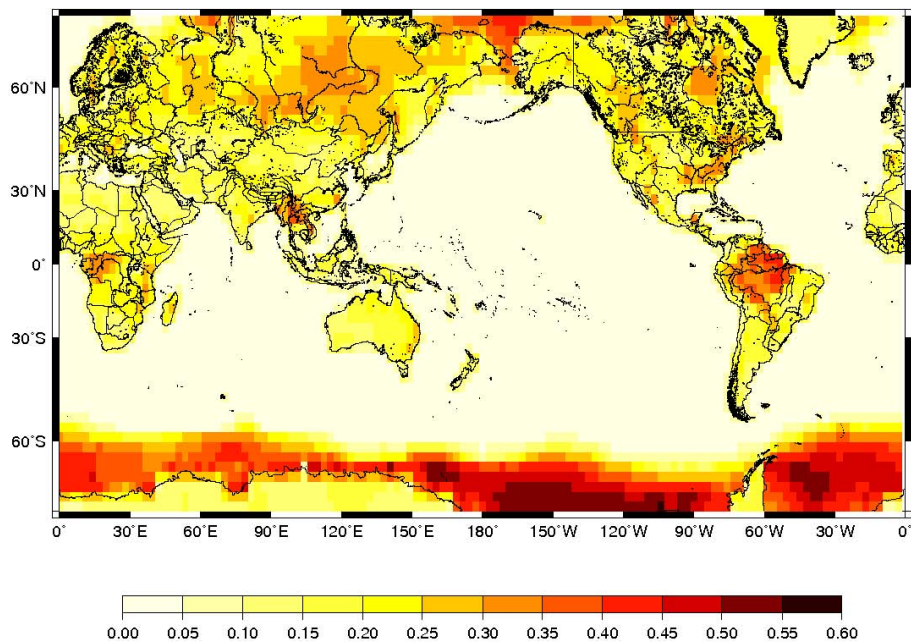
Fig. 4. Mean annual O_3 deposition velocity [$cm\,s^{-1}$].
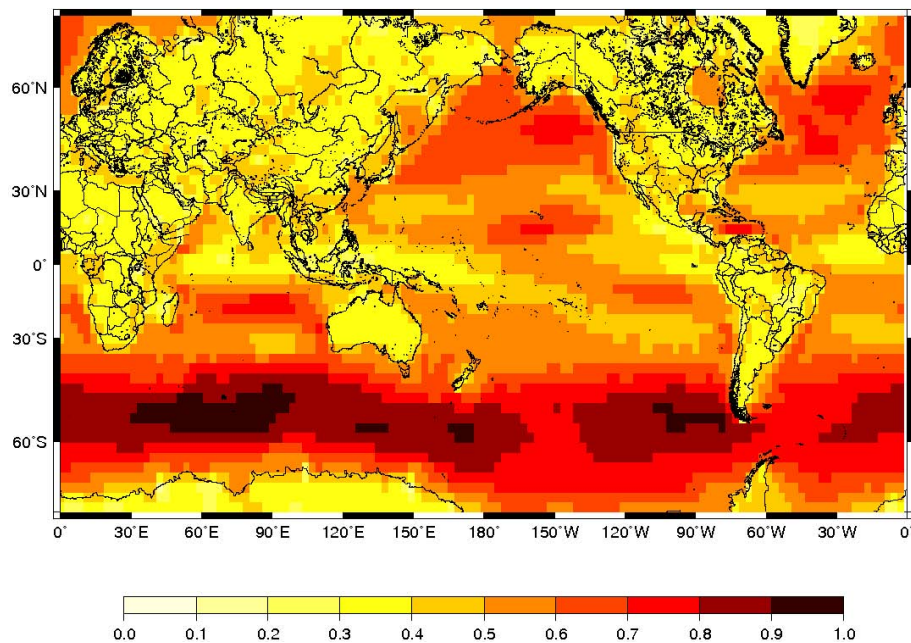
Fig. 5. Mean annual SO_2 deposition velocity [$cm\,s^{-1}$].

Full Screen / Esc

Printer-friendly Version

Interactive Discussion
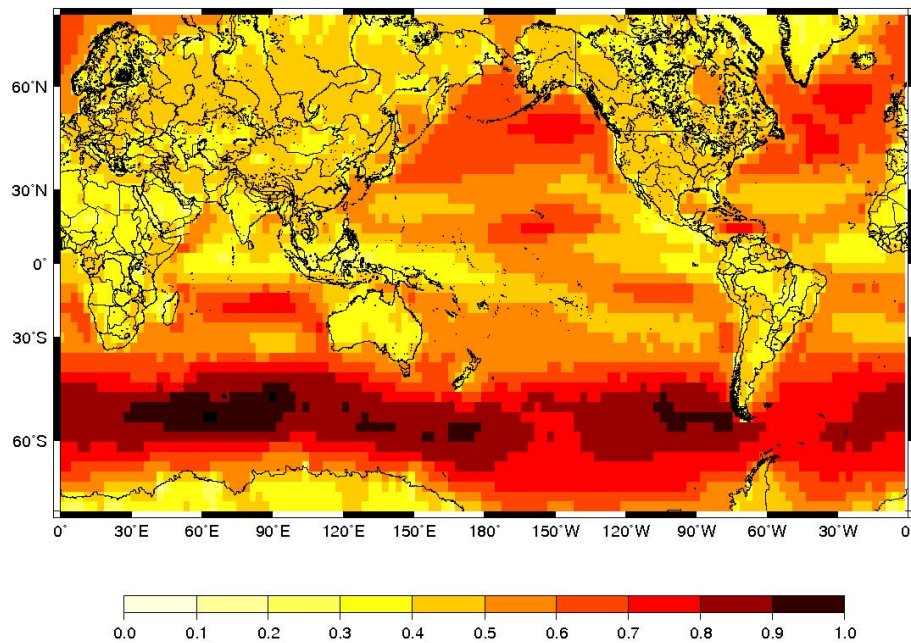
Fig. 6. Mean annual RGM deposition velocity [cm s^{-1}].

ECHMERIT model

G. Jung et al.
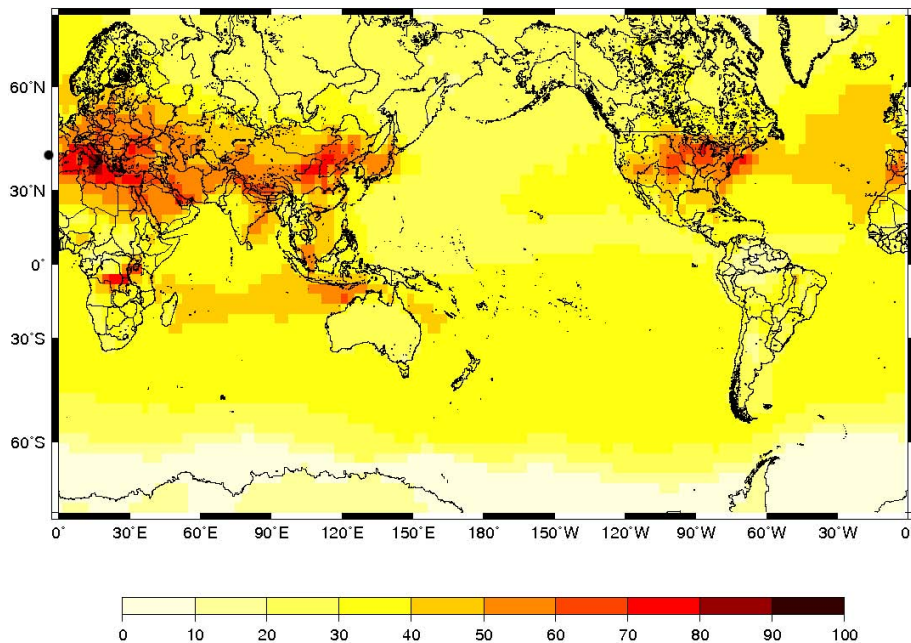
Fig. 7. Mean simulated summer (JJA) surface layer ozone concentration [ppb].

Printer-friendly Version

Interactive Discussion
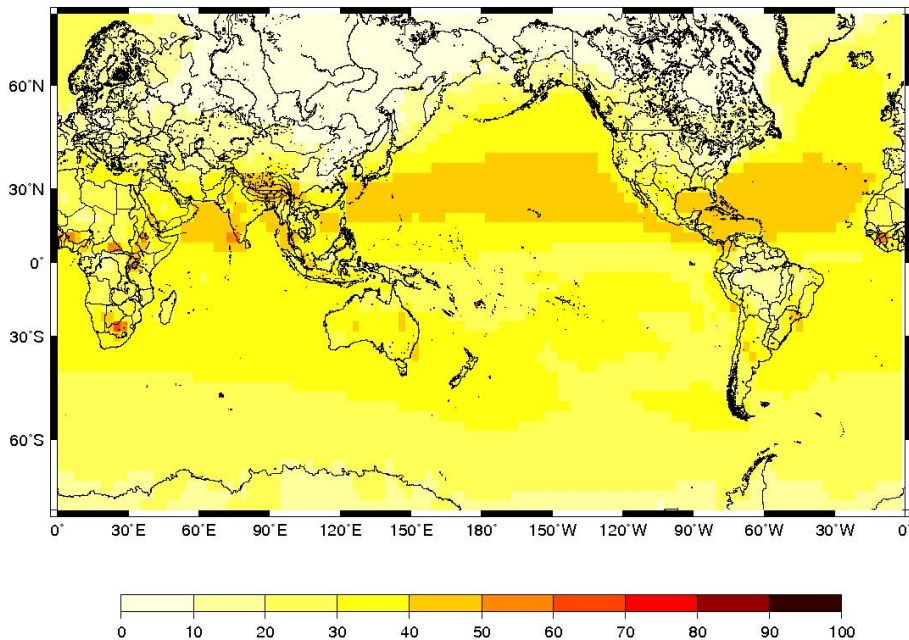
Fig. 8. Mean simulated winter (DJF) surface layer ozone concentration [ppb].
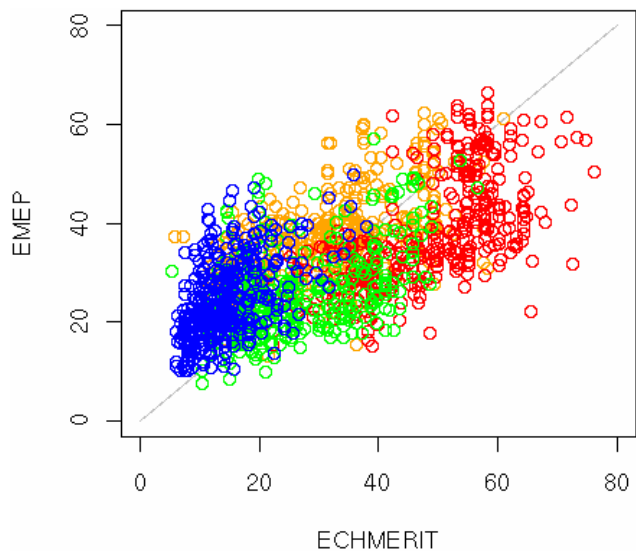
Fig. 9. Simulated vs. observed (EMEP) monthly mean ozone concentration [ppb], colours mark different seasons: red=JJA, orange=MAM, green=SON, blue=DJF.
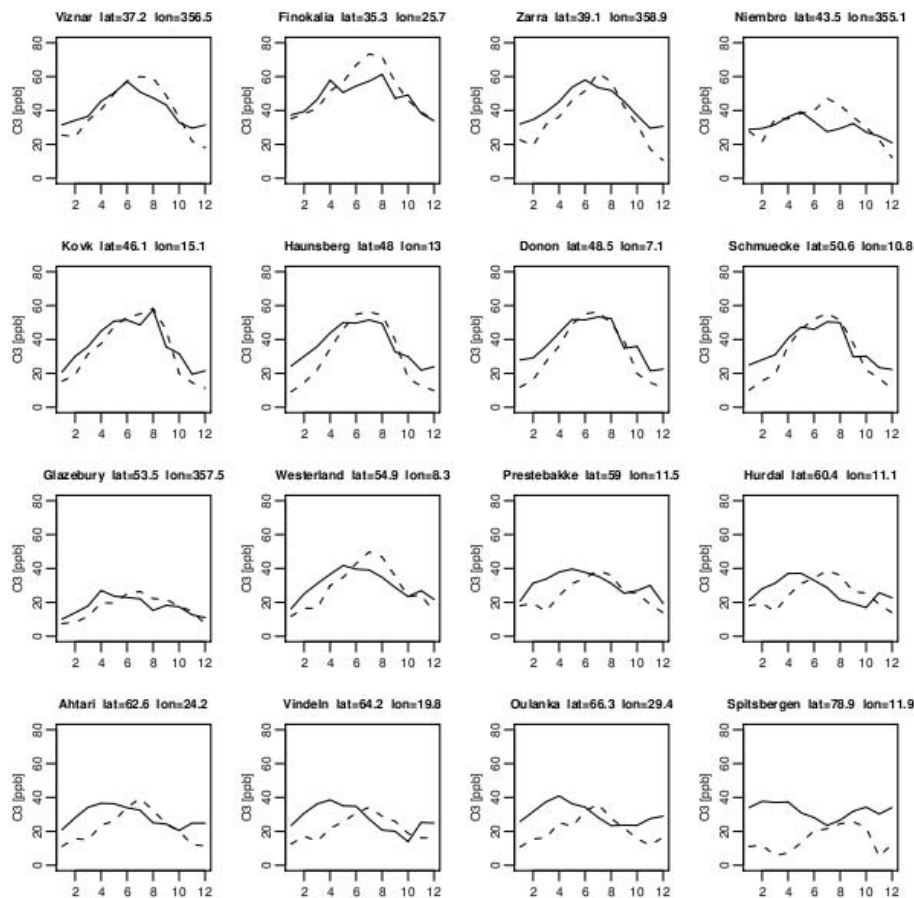
Fig. 10. Simulated vs. observed (EMEP) monthly mean ozone concentrations [ppb] for selected observational stations, dashed: ECHMERIT, full line: EMEP observations.
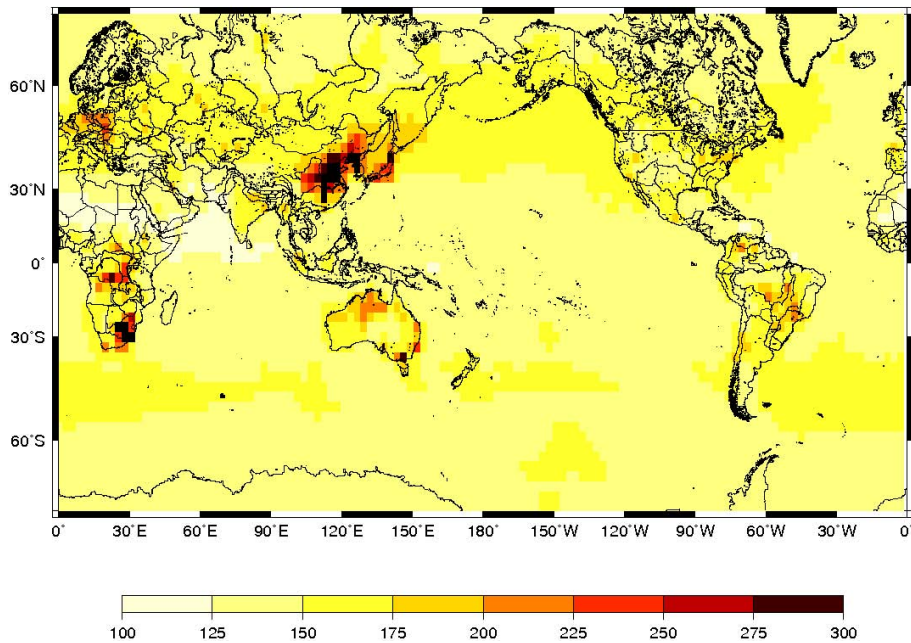
Fig. 11. Annual mean simulated surface layer TGM concentration [ppq].
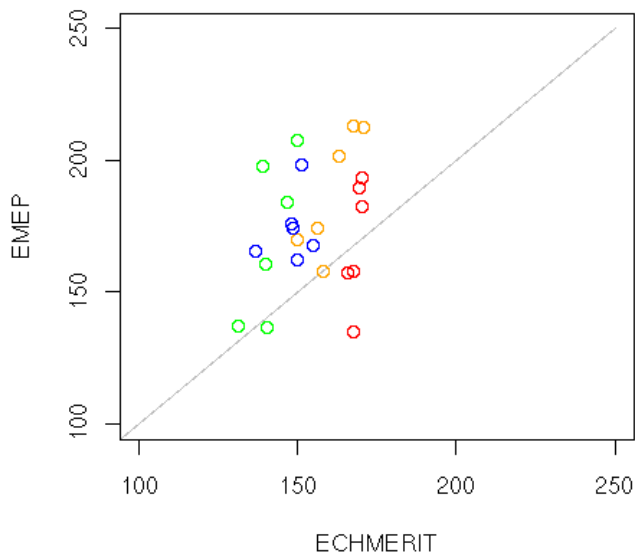
Fig. 12. Simulated vs. observed (EMEP) monthly mean TGM concentration [ppq], colors mark different seasons: red=JJA, orange=MAM, green=SON, blue=DJF.
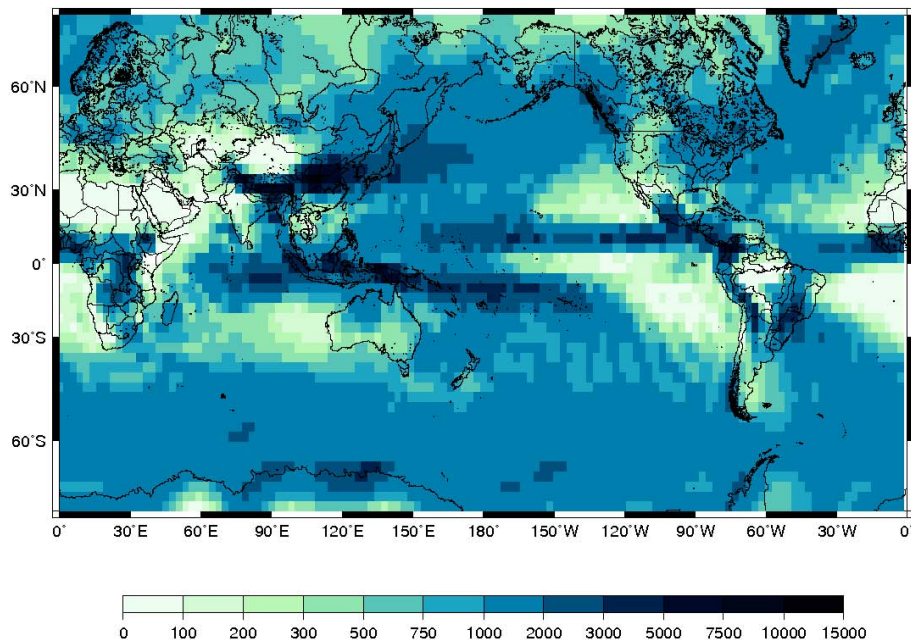
Fig. 13. Annual precipitation [mm].
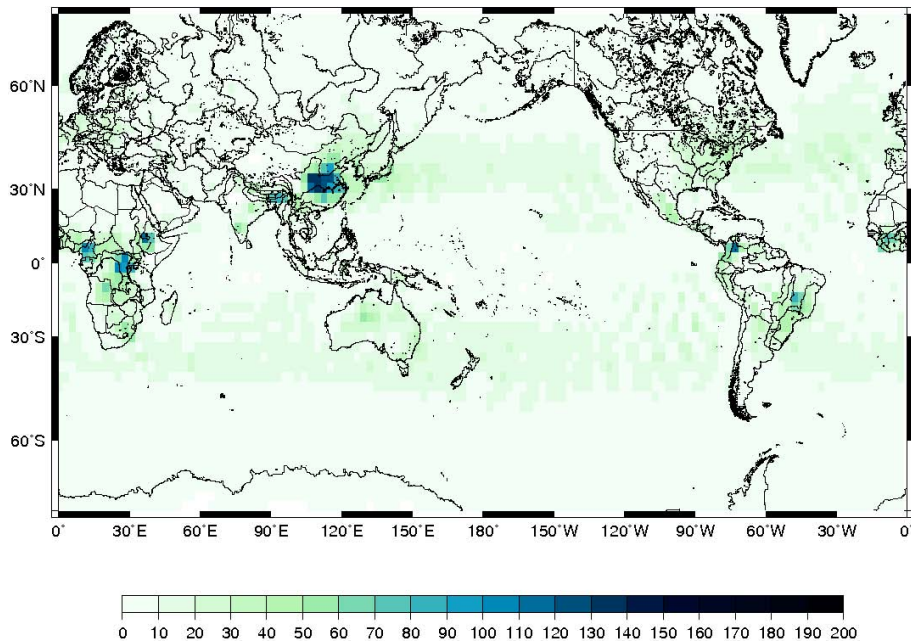
Fig. 14. Annual Hg wet deposition [μg m^{-2}].

ECHMERIT model

G. Jung et al.
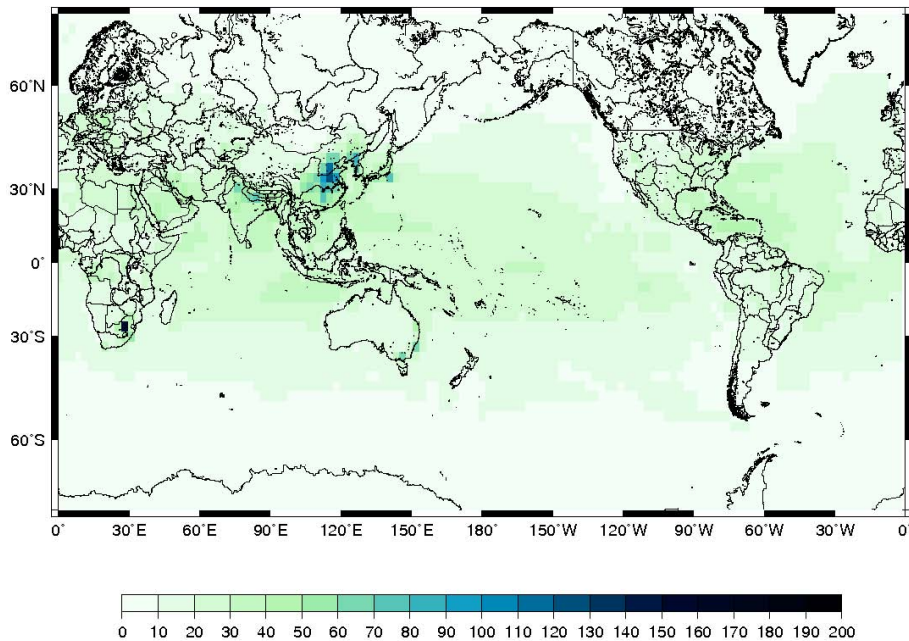
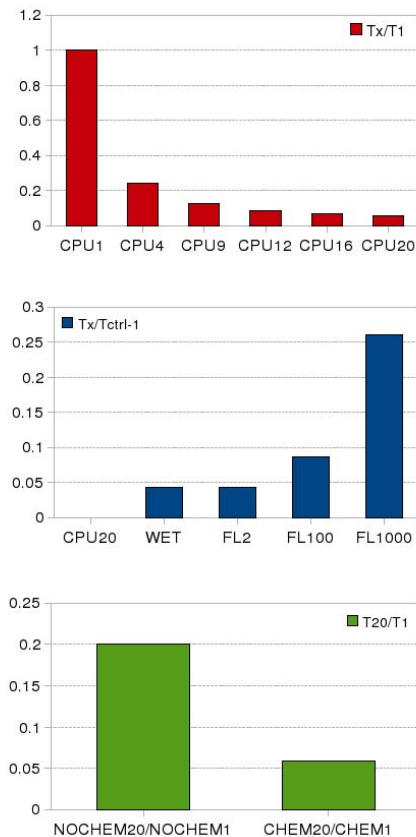**Fig. 15.** Annual Hg dry deposition [μg m^{-2}].

Fig. 16. Model perfomance; top: for different numbers of processors with respect to 1 cpu, middle: for different chemical schemes (dry and wet with different representations of droplet spectrum), bottom: advantage of cpu number ECHMERIT and ECHAM5.